The Astrophysical Journal, 794:143 (19pp), 2014 October 20 doi:10.1088/0004-637X/794/2/143

SpeX SPECTROSCOPY OF UNRESOLVED VERY LOW MASS BINARIES. II. IDENTIFICATION OF 14 CANDIDATE BINARIES WITH LATE-M/EARLY-L AND T DWARF COMPONENTS

Daniella C. Bardalez Gagliuffi[1,12], Adam J. Burgasser[1,12], Christopher R. Gelino[2,3], Dagny L. Looper[4,12], Christine P. Nicholls[1,5], Sarah J. Schmidt[6,12], Kelle Cruz[7,8], Andrew A. West[9], John E. Gizis[10], and Stanimir Metchev[11]
[1] Center for Astrophysics and Space Sciences, University of California, San Diego, 9500 Gilman Drive, Mail Code 0424, La Jolla, CA 92093, USA; daniella@physics.ucsd.edu
[2] NASA Exoplanet Science Institute, Mail Code 100-22, California Institute of Technology, 770 South Wilson Avenue, Pasadena, CA 91125, USA
[3] Tisch School of the Arts, New York University, 721 Broadway, New York, NY 10003, USA
[4] School of Mathematics and Physics, The University of Queensland, Brisbane, QLD 4072, Australia
[5] Department of Astronomy, Ohio State University, 140 West 18th Avenue, Columbus, OH 43210, USA
[6] Department of Physics and Astronomy, Hunter College, City University of New York, 695 Park Avenue, New York, NY 10065, USA
[7] Department of Astrophysics, American Museum of Natural History, Central Park West at 79th Street, New York, NY 10024, USA
[8] Department of Astronomy, Boston University, CAS 422A, 725 Commonwealth Avenue, Boston, MA 02215, USA
[9] Department of Physics and Astronomy, University of Delaware, 104 The Green, Newark, DE 19716, USA
[10] Department of Physics and Astronomy, Western University, London, ON N6A 3K7, Canada
[11] Infrared Processing and Analysis Center, Mail Code 100-22, California Institute of Technology, 1200 East California Boulevard, Pasadena, CA 91125, USA
Received 2014 May 19; accepted 2014 August 12; published 2014 October 2

ABSTRACT

Multiplicity is a key statistic for understanding the formation of very low mass (VLM) stars and brown dwarfs. Currently, the separation distribution of VLM binaries remains poorly constrained at small separations ($\leqslant$1 AU), leading to uncertainty in the overall binary fraction. We approach this problem by searching for late-M/early-L plus T dwarf spectral binaries whose combined light spectra exhibit distinct peculiarities, allowing for separation-independent identification. We define a set of spectral indices designed to identify these systems, and we use a spectral template fitting method to confirm and characterize spectral binary candidates from a library of 815 spectra from the SpeX Prism Spectral Libraries. We present 11 new binary candidates, confirm 3 previously reported candidates, and rule out 2 previously identified candidates, all with primary and secondary spectral types in the range M7–L7 and T1–T8, respectively. We find that subdwarfs and blue L dwarfs are the primary contaminants in our sample and propose a method for segregating these sources. If confirmed by follow-up observations, these systems may add to the growing list of tight separation binaries, whose orbital properties may yield further insight into brown dwarf formation scenarios.

Key words: binaries: close – binaries: general – brown dwarfs – stars: low-mass

Online-only material: color figures, machine-readable table

1. INTRODUCTION

Brown dwarfs are self-gravitating objects with physical and atmospheric properties intermediate between stars and planets. With masses below $\simeq$0.075 $M_\odot$ (Kumar 1963; Hayashi & Nakano 1963),[13] these objects cannot sustain hydrogen fusion, and hence they cool and dim as they age, radiating primarily at infrared wavelengths. The evolution of their spectra spans the spectral classes M, L, T, and Y, with transitions demarcated by the appearance and disappearance of absorption lines and bands as molecules form and condense out of their atmospheres at different temperatures and pressures (Kirkpatrick 2005 and references therein).

Despite having a basic understanding of their evolution, brown dwarf formation remains an open question. Standard Jeans collapse of molecular clouds requires high densities so that gravity can overcome thermal pressure. Once the collapse has begun, halting the accretion becomes problematic (Shu et al. 1987). Several mechanisms have been proposed to resolve this issue, including turbulent fragmentation of protostellar clouds (Padoan & Nordlund 2002), fragmentation of prestellar disks (Stamatellos & Whitworth 2009), ejection by dynamical interactions with other protostars (Reipurth & Clarke 2001), and photoerosion of prestellar cores (Whitworth & Zinnecker 2004). In principle, these formation mechanisms should leave traces on the statistical properties of brown dwarfs, including the occurrence of multiple systems and distributions of their separation, relative masses, and eccentricity.

Observationally, it has been shown that multiplicity increases with primary mass, even at the lower mass end of the main sequence, with the G dwarf binary fraction being 57% higher than that for M dwarfs (Fischer & Marcy 1992; Delgado-Donate et al. 2004). Current estimates of the binary fraction of very low mass (VLM) late-M to T dwarfs (VLM $M_{\rm total} < 0.1\,M_\odot$) are 20%–25%, with a peak in separation at $\sim$4 AU and a mass ratio distribution peaking at nearly equal masses (Bouy et al. 2003; Close et al. 2003; Burgasser et al. 2006b; Allen 2007; Kraus & Hillenbrand 2012). However, these multiplicity statistics have been largely determined from resolved imaging programs, sampling separations greater than 3 AU. Burgasser et al. (2007b) pointed out that the current peak in the binary angular separation distribution is coincident with the resolution limit of *Hubble Space Telescope* (*HST*) and ground-based

[12] Visiting Astronomer at the Infrared Telescope Facility, which is operated by the University of Hawaii under Cooperative Agreement no. NNX-08AE38A with the National Aeronautics and Space Administration, Science Mission Directorate, Planetary Astronomy Program.
[13] Minimum mass for hydrogen fusion may vary between 0.072 and 0.078 $M_\odot$ depending on age and metallicity. See Burrows et al. (1997) for an extensive discussion of evolutionary models.

adaptive optics (AO) imaging, indicating that tight (<1 AU) VLM binaries could be undercounted. Likewise, Pinfield et al. (2003) and Chappelle et al. (2005) report a higher unresolved binary fraction (30%–50%) based on overluminous binary candidates in color–magnitude plots. Conversely, spectroscopic radial velocity (RV) studies find binary fractions of 2.5% in systems separated by <1 AU (Blake et al. 2010) and 2%–28% up to 3 AU (Joergens 2008). For the 0–6 AU range, Basri & Reiners (2006) estimate a binary fraction of 26% ± 10%. However, the difficulty of obtaining high-resolution spectra of faint VLM dwarfs results in a small sample size. Since total binary fractions for VLM stars and brown dwarfs could range between 2% and 50%, it is imperative to constrain this statistic to make conclusions about brown dwarf formation.

An alternative method for detecting tight unresolved binaries, developed by Burgasser (2007a), involves identifying blended light pairs, or spectral binaries. We will refer to *spectral* binaries as those objects whose combined-light spectrum shows distinct peculiarities that come from the highly structured spectra of single M, L, and T dwarfs when blended together, as opposed to *spectroscopic* binaries, which are binaries that show RV variations. The first brown dwarf spectral binary, 2MASS J05185995−2828372, was serendipitously identified by Cruz et al. (2004) based on its hybrid characteristics containing features of both L and T dwarfs. The superposition of L plus T dwarf spectra proved to be the simplest model of its peculiar spectrum, and it was later resolved as a binary using *HST* (Burgasser et al. 2006b). The unusually blue L dwarf SDSS J080531.84+481233.0 was next identified as a spectral binary with L4.5 and T5 components by Burgasser (2007b), based on a peculiar methane absorption band starting at 1.60 μm, and was later confirmed as an astrometric variable by Dupuy & Liu (2012). A third system, 2MASS J03202839−0446358, was concurrently identified as an unresolved M9+T5 spectral binary (Burgasser et al. 2008a) and an RV variable with an orbital period of 8 months (Blake et al. 2008). These examples serve to illustrate how spectral binaries can encompass a broad range of system architectures. To date, 34 VLM spectral binaries and candidates have been reported (see Table 1), and 10 have been confirmed by direct imaging, RV, or astrometric variability (Burgasser et al. 2011a; Stumpf et al. 2011; Burgasser et al. 2012; Dupuy & Liu 2012; Faherty et al. 2012; Manjavacas et al. 2013; D. Bardalez Gagliuffi et al., in preparation).

Detecting binaries using the spectral binary method is particularly useful for multiplicity statistics, as the method is independent of separation within 0.″5, which translates to <10–20 AU for field brown dwarfs at distances of 20–40 pc. The closest separation pairs can be followed up to measure orbits and component masses, as well as infer ages by comparison to evolutionary models (Burgasser & Blake 2009). Systems with independent age constraints can also be used to test the evolutionary models directly (Dupuy et al. 2009; Liu et al. 2010; Burgasser et al. 2011a). Additionally, unresolved binaries are strong contaminants in luminosity functions that later lead to uncertainties in mass functions and studies of formation history through stellar populations (Day-Jones et al. 2013), so their identification is extremely important. Finally, spectral binaries with late-M/early-L primaries and T dwarf secondaries can straddle the hydrogen-burning limit, thus giving additional insight into brown dwarf evolution.

In this paper we adapt the technique of Burgasser et al. (2010a) to search for spectral binaries composed of late-M or early-L dwarf primaries with T dwarf secondaries. M dwarfs are the most common stars in the galaxy (Bochanski et al. 2010) and are the brightest VLM objects, enabling better statistics through larger magnitude-limited search volumes and sample sizes. M-dwarf spectra are also intrinsically distinct from T-dwarf spectra, but they differ in brightness by several magnitudes, rendering peculiar features extremely subtle. In Section 2 we describe our spectral sample used to find spectral binaries, drawn from the SpeX Prism Libraries and new observations. In Section 3 we explain our two methods to identify spectral binary candidates: by visual examination (Section 3.1) and through spectral indices (Section 3.2). In Section 3.3 we perform single and binary template fitting to identify 14 binary candidates. In Section 4 we describe the properties of the candidates. In Section 5.1 and Section 5.2 we discuss our major contaminant, blue L dwarfs, and show preliminary evidence that the separations of spectral binaries are tighter than the resolved population. Our results are summarized in Section 6.

2. SpeX SPECTRAL SAMPLE

The SpeX Prism Library is composed of low-resolution ($\lambda/\Delta\lambda$ = 75–120) spectra acquired with the SpeX 0.8–2.5 μm spectrograph, mounted on the 3.0 m NASA Infrared Telescope Facility (IRTF), located in Mauna Kea, HI (Rayner et al. 2003). All spectra were obtained using the prism-dispersed SpeX mode, which continuously samples wavelengths between 0.75 and 2.5 μm at a dispersion of 20–30 Å pixel^{-1}. The library includes close to 2000 sources, both previously published data (e.g., Burgasser et al. 2010a; Chiu et al. 2006; Cruz et al. 2003) and 530 new spectra acquired between 2000 November and 2013 December (Table 2). The new observations were obtained with the 0.″5 or 0.″7 slit, generally aligned with the parallactic angle. Total integration times ranged between 360 s and 1200 s, depending on source brightness and atmospheric conditions, and were obtained in an ABBA dither pattern along the slit. Spectra of nearby A0V stars were used to flux-calibrate the raw spectra and correct for telluric absorption. Internal flat fields and argon arc lamps were observed with each flux standard for pixel response and wavelength calibration. All data were reduced with the SpeXtool package (Cushing et al. 2004; Vacca et al. 2003) using standard settings. A detailed description of our reduction procedures is given in Burgasser (2007b).

The sources observed have optical and/or near-infrared (NIR) spectral classifications reported in the literature. To obtain a self-consistent set of spectral types, we computed SpeX spectral types based on spectral indices, following the method described in Burgasser (2007a). From these, we selected two samples: the "candidate" sample, which has been purged of spectral types outside the M7–L7 range, optical subdwarfs, giants, and poor-quality spectra, but keeping binaries, objects suspected of being binaries from previous studies, young objects, and unusually red and blue dwarfs, and the "template" sample, which has been purged of binaries, candidate binaries, giants, and poor-quality spectra (as determined by visual inspection) only. The "candidate" sample contains 815 spectra of 738 objects with SpeX spectral types between M7 and L7, as those would be the potential primaries for late-M/early-L plus T binaries. The "template" sample comprises 1110 spectra of 992 single sources whose spectral types range between M7 and L7 for primaries and between T1 and T8 for secondaries used in spectral fitting.

Table 1
Compilation of All Confirmed and Candidate Spectral Binaries Discovered to Date

Name	Spectral Type				J (mag)	$J-K_s$	ΔJ	Separation[a]	Confirmation[b]	Ref.
	Optical	NIR	Primary	Secondary				(AU)	method	SB; Conf.
SDSS J000649.16-085246.3[c, d]	M9	···	M8.5 ± 0.5	T5 ± 1	14.14 ± 0.04	1.01 ± 0.05	3.15 ± 0.31	0.29 ± 0.01	RV	2; 2
ULAS J004757.41+154641.4	···	T2.0 ± 2.0	L8.0	T7.0	17.83 ± 0.05	1.41 ± 0.07	···	<65		22
2MASS J00521232+0012172	L5	···	L4	T3	16.36 ± 0.11	0.90 ± 0.19	···	<49		24
SDSS J011912.22+240331.6	···	T2	T0 ± 0.7	T4 ± 0.4	17.02 ± 0.18	< − 0.02	−0.42 ± 0.19	<43		21
ULAS J020529.62+142114.0	···	T1.0 ± 0.5	T1.0	T3.0	17.99 ± 0.04	1.06 ± 0.07	···	<71		22
2MASS J02060879+22355930	···	L5.5	L5.1 ± 0.5	T3.2 ± 2.3	16.56 ± 0.11	1.39 ± 0.17	1.61 ± 0.89			26
2MASS J02361794+0048548	L6.5	···	L5.0 ± 0.6	T1.9 ± 1.1	16.10 ± 0.08	1.43 ± 0.12	1.05 ± 0.48	<48		26
SDSS J024749.90-163112.6	···	T2.0 ± 1.5	T0 ± 0.2	T7 ± 0.3	17.19 ± 0.18	1.57 ± 0.27	0.68 ± 0.10	<36		21
2MASS J03202839-0446358[c, d]	M8:	L1	M8.5 ± 0.3	T5 ± 0.9	12.13 ± 0.03	1.13 ± 0.04	3.5 ± 0.2	<0.58	RV	5; 1
SDSS J035104.37+481046.8	···	T1.0 ± 1.5	L6.5 ± 0.7	T5 ± 0.7	16.47 ± 0.13	1.47 ± 0.18	0.31 ± 0.31	<34		21
DENIS-P J04272708-1127143	···	dM7	M7.4 ± 0.2	T5.1 ± 1.5	13.74	0.99 ± 0.14	4.13 ± 0.62			26
2MASS J05185995-2828372[d]	···	···	L6	T4	15.98 ± 0.10	1.82 ± 0.12	0.13 ± 0.19	1.80 ± 0.50	DI	10; 7
2MASS J07354882+2720167	L1	···	L1	L4	16.94 ± 0.13	1.28 ± 0.21	···	<112		23
SDSS J080531.84+481233.0[c, d]	L4	L9.5	L4.5	T5	14.73 ± 0.04	1.46 ± 0.05	1.50 ± 0.09	0.9-2.3	AV	6; 11
SDSS J090900.73+652527.2	···	T1.5	T1.5 ± 0.5	T2.5 ± 0.3	16.03 ± 0.09	0.86 ± 0.17	−0.12 ± 0.10	<29		21
SDSS J092615.38+584720.9	T4.5	···	T3	T6	16.77 ± 0.14	<1.57	0.4 ± 0.2[e]	2.6 ± 0.5	DI	16; 7, 8
SDSS J093113.23+280227.1	L3	···	L1.4 ± 0.1	T2.6 ± 0.9	14.98 ± 0.04	1.25 ± 0.06	2.22 ± 0.23	<37		26
2MASS J09490860-1545485	···	T2	T1 ± 0.2	T2 ± 0.2	16.15 ± 0.12	0.92 ± 0.20	−0.07 ± 0.05	<25		21
2MASS J10365305-3441380	L6	···	L5.2 ± 0.4	T1.4 ± 0.4	15.62 ± 0.05	1.82 ± 0.06	0.51 ± 0.32	<30		26
SDSS J103931.35+325625.5	···	T1	L7 ± 0.2	T4 ± 0.2	16.41 ± 0.15	1.25 ± 0.22	0.26 ± 0.09	<34		21
2MASS J10595138-2113082	L1	···	L0.6 ± 0.4	T3.4 ± 1.3	14.56 ± 0.04	1.35 ± 0.06	2.58 ± 0.32	<52.5		26
2MASS J11061197+2754225[d]	···	T2.5	T0 ± 0.2	T4.5 ± 0.2	14.82 ± 0.04	1.02 ± 0.07	−0.37 ± 0.06	<2.67	OL	4, 14; 15
SDSS J120747.17+024424.8	L8	T0	L6.5 ± 0.7	T2.5 ± 0.5	15.58 ± 0.07	1.59 ± 0.09	0.48 ± 0.28	<17		21
2MASS J12144089+6316434	···	T3.5	T2	T6	16.59 ± 0.12	0.71 ± 0.26	···	<24		24
2MASS J13114227+3629235	L5pec	···	L4.8 ± 0.6	T4.1 ± 2.7	15.54 ± 0.05	1.40 ± 0.09	2.19 ± 1.02	<27		27
2MASS J13153094-2649513[c, d]	L5	···	L3.5 ± 2.5	T7 ± 0.6	15.07 ± 0.05	1.63 ± 0.07	3.03 ± 0.03	6.60 ± 0.90	DI	3; 3
2MASS J13243559+6358284	···	T2:	L8 ± 0.2	T3.5 ± 0.2	15.60 ± 0.07	1.54 ± 0.09	−0.05 ± 0.06	<23		21, 2 4
2MASS J13411160-30525049	L3	···	L1.2 ± 0.3	T6.3 ± 1.0	14.61 ± 0.03	1.53 ± 0.04	3.28 ± 0.53	<39		26
SDSS J141530.05+572428.7	···	T3 ± 1	L8 ± 0.5	T5 ± 0.3	16.73 ± 0.16	<1.19	−0.13 ± 0.20	<29		21
SDSS J142227.20+221557.5	L6.5	···	L4.2 ± 0.6	T4.1 ± 2.3	16.87 ± 0.03	1.23 ± 0.04	2.36 ± 0.78	<43		26
SDSS J143553.25+112948.6	···	T2 ± 1	L7.5 ± 0.4	T6 ± 0.3	17.14 ± 0.23	<0.23	0.41 ± 0.12	<39		21
SDSS J143945.86+304220.6	···	T2.5	T1 ± 0.2	T5 ± 0.6	17.22 ± 0.23	<1.34	0.06 ± 0.24	<45		21
2MASS J14532589+1420418	L1	···	L1.1 ± 0.0	T6.0 ± 1.1	15.07 ± 0.04	1.18 ± 0.05	3.27 ± 0.46	<72		26
SDSS J151114.66+060742.9[d]	···	T0 ± 2	L5.5 ± 0.8	T5 ± 0.4	16.02 ± 0.08	1.47 ± 0.13	0.54 ± 0.32	<21	OL	4; 12
SDSS J151603.03+025928.9	···	T0:	L7.5 ± 1.1	T2.5 ± 2.2	17.23 ± 0.20	1.80 ± 0.27	0.30 ± 0.65	<27		21, 24
WISE J16235970-0508114	···	L1	L0.6 ± 0.3	T6.0 ± 0.8	14.94 ± 0.04	1.39 ± 0.06	3.39 ± 0.40			26
2MASS J17072529-0138093	···	···	L0.7 ± 0.5	T4.3 ± 2.0	14.29 ± 0.03	1.22 ± 0.04	2.87 ± 0.75	<31		26
2MASSI J17114573+2232044	L6.5	···	L1.5 ± 0.6	T2.5 ± 1.0	17.09 ± 0.18	2.36 ± 0.20	1.20 ± 0.40	<35		21
2MASS J17310140+5310476	L6	···	L5	L8	16.37 ± 0.11	1.52 ± 0.18	···	<48		23, 24

Table 1
(Continued)

Name	Spectral Type				J (mag)	$J - K_s$	ΔJ	Separation[a]	Confirmation[b]	Ref.
	Optical	NIR	Primary	Secondary				(AU)	method	SB; Conf.
2MASS J17373467+5953434	L9	···	L5	T5	16.88 ± 0.16	1.16 ± 0.31	···	<50		23
2MASS J20261584-2943124	L1:	···	L0.1 ± 0.5	T5.8 ± 1.0	14.80 ± 0.03	1.44 ± 0.05	3.42 ± 0.40	<9.00	DI	13
SDSS J205235.31-160929.8[d]	···	T1 ± 1	L7.5 ± 0.6	T2 ± 0.2	16.33 ± 0.12	1.21 ± 0.19	0.04 ± 0.18	3.20 ± 0.50	DI	4; 17
2MASS J21265916+7617440	L7	T0	L7	T3.5	14.34 ± 0.03	1.18 ± 0.05	···			28
2MASS J21392676+0220226	···	T1.5	L8.5 ± 0.7	T3.5 ± 1.0	15.26 ± 0.05	1.68 ± 0.07	−0.14 ± 0.21	<14		21
ULAS J222958.30+010217.2	···	T3.0 ± 0.5	T1.0	T5.0	17.89 ± 0.04	0.67 ± 0.10	···	<62		22
ULAS J223348.82+002214.0	···	T0.0 ± 0.5	L5.0	T4.0	18.07 ± 0.05	1.43 ± 0.07	···	<90		22
ULAS J235618.01+075420.4	···	T0.0 ± 1.0	L7.0	T7.0	18.09 ± 0.05	1.87 ± 0.06	···	<58		22
ULAS J232315.39+071931.0	···	T2.0 ± 0.5	T0.0	T2.0	17.30 ± 0.02	1.01 ± 0.04	···	<49		22
Kelu-1A	L3pec ± 1.5	L2.0 ± 1.0	L0.5 ± 0.5	T7.5 ± 1	13.88 ± 0.03	1.57 ± 0.04	···	$6.4^{+2.4}_{-1.3}$		25

Notes.
[a] Upper limits based on SDSS angular resolution (1″; York et al. 2000) and distance reported or estimated from absolute magnitudes (Looper et al. 2008a).
[b] RV, radial velocity; DI, direct imaging; AV, astrometric variability; OL, overluminous.
[c] Used as M+T binary benchmark.
[d] Spectral binaries with confirmed separations. See Figure 6.
[e] Estimated from F110W filter (Burgasser et al. 2006b).

References. (1) Blake et al. 2008; (2) Burgasser et al. 2012; (3) Burgasser et al. 2011b; (4) Burgasser et al. 2010a; (5) Burgasser et al. 2008a; (6) Burgasser 2007b; (7) Burgasser et al. 2006b; (8) Carson et al. 2011; (9) Chiu et al. 2006; (10) Cruz et al. 2004; (11) Dupuy & Liu 2012; (12) Faherty et al. 2012; (13) Gelino & Burgasser 2010; (14) Looper et al. 2008a; (15) Manjavacas et al. 2013; (16) Metchev et al. 2008; (17) Stumpf et al. 2011; (21) Burgasser et al. 2010a; (22) Day-Jones et al. 2013; (23) Geißler et al. 2011; (24) Metchev et al. 2008; (25) Stumpf et al. 2008; (26) this paper; (27) Kirkpatrick et al. 2011; (28) Kirkpatrick et al. 2010.

Table 2
New SpeX Observations of M7–L6 Dwarfs

Source	Designation	Spectral Type			2MASS		Date	$\lambda/\Delta\lambda$	Ref[b]
		Opt	NIR	SpeX[a]	J	$J-K_s$			
2MASS J0000286-124515	J00002867-1245153	M8.5	···	M9.2	13.20	1.23	2013 Aug 14	120	44; 44
LEHPM 1-162	J00054768-2157176	M8.5	M8	M8.7	13.27	1.07	2006 Sep 03	120	32; 75
2MASSI J0006205-172051	J00062050-1720506	L2.5	···	L3.0	15.66	1.65	2008 Sep 08	120	25; 25
SDSS J000632.60+140606.4	J00063260+1406064	L1	···	L0.4	15.85	0.79	2009 Jun 30	120	48; 48
SDSS J000646.81+151225.8	J00064681+1512258	L4::	···	L4.3	16.22	1.41	2013 Sep 03	120	62; 62
2MASS J0007078-245804	J00070787-2458042	M7	···	M7.7	13.12	1.05	2013 Oct 23	120	44; 44
2MASS J00100009-2031122	J00100009-2031122	L0	···	M8.8:	14.13	1.25	2008 Jul 14	120	44; 44
2MASSI J0013578-223520	J00135779-2235200	L4	···	L5.7	15.78	1.74	2009 Nov 04	120	25; 25
2MASSW J0015447+351603	J00154476+3516026	L2	···	L1.0	13.88	1.61	2008 Sep 08	120	13; 13
SDSS J001608.44-004302.3	J00160843-00430209	···	L5.5	L4.3	16.33	1.78	2013 Sep 03	120	34; 34

Notes.
[a] NIR classification from SpeX data based on index method described in Burgasser (2007a).
[b] First citation is the discovery reference; next citation(s) are classification references (optical and NIR).
References. (1) Haro & Chavira 1966; (2) Liebert 1976; (3) Becklin & Zuckerman 1988; (4) Bessell 1991; (5) Kirkpatrick et al. 1995; (6) Tinney et al. 1998; (7) Rebolo et al. 1998; (8) EROS Collaboration et al. 1999; (9) Delfosse et al. 1999; (10) Martín et al. 1999; (11) Kirkpatrick et al. 1999; (12) Fan et al. 2000; (13) Kirkpatrick et al. 2000; (14) Gizis et al. 2000b; (15) Basri et al. 2000; (16) Gizis et al. 2000a; (17) Scholz et al. 2001; (18) Wilson et al. 2001; (19) Schneider et al. 2002; (20) Hawley et al. 2002; (21) Geballe et al. 2002; (22) Gizis 2002; (23) Lépine et al. 2002; (24) Phan-Bao et al. 2003; (25) Kendall et al. 2003; (26) Lépine et al. 2003; (27) Cruz et al. 2003; (28) Cruz et al. 2003; (29) Berriman et al. 2003; (30) Wilson et al. 2003; (31) Kendall et al. 2004; (32) Pokorny et al. 2004; (33) Scholz et al. 2004; (34) Knapp et al. 2004; (35) Golimowski et al. 2004; (36) Deacon et al. 2005; (37) Lodieu et al. 2005; (38) Billères et al. 2005; (39) Reid & Gizis 2005; (40) Chiu et al. 2006; (41) McElwain & Burgasser 2006; (42) Cushing et al. 2006; (43) Liebert & Gizis 2006; (44) Cruz et al. 2007; (45) Burgasser et al. 2007a; (46) Caballero 2007; (47) Kendall et al. 2007; (48) West et al. 2008; (49) Reid et al. 2008; (50) Burgasser et al. 2008b; (51) Looper et al. 2008b; (52) Kirkpatrick et al. 2008; (53) Phan-Bao et al. 2008; (54) Zhang et al. 2009; (55) Faherty et al. 2009; (56) Cruz et al. 2009; (57) Shkolnik et al. 2009; (58) Jenkins et al. 2009; (59) Martín et al. 2010; (60) Schmidt et al. 2010; (61) Kirkpatrick et al. 2010; (62) Zhang et al. 2010; (63) Bochanski et al. 2011; (64) Phan-Bao 2011; (65) Geißler et al. 2011; (66) Kirkpatrick et al. 2011; (67) Shkolnik et al. 2012; (68) Folkes et al. 2012; (69) Thompson et al. 2013; (70) Scholz 2014; (71) Allers & Liu 2013; (72) Andrei et al. 2011; (73) Boeshaar & Tyson 1985; (74) S. Schmidt et al. (in preparation); (75) this paper; (76) Cruz et al. 2013; (77) Deacon et al. 2009; (78) Forveille et al. 2004; (79) Hall 2002; (80) Irwin et al. 1991; (81) J. D. Kirkpatrick (private communication); (82) Kendall et al. 2007; (83) Lodieu et al. 2002; (84) D. Looper et al. (in preparation); (85) Phan-Bao 2011; (86) Radigan et al. 2008; (87) Ruiz & Takamiya 1995; (88) Salim et al. 2003; (89) Tinney et al. 1993; (90) van Biesbroeck 1961.

(This table is available in its entirety in a machine-readable form in the online journal. A portion is shown here for guidance regarding its form and content.)

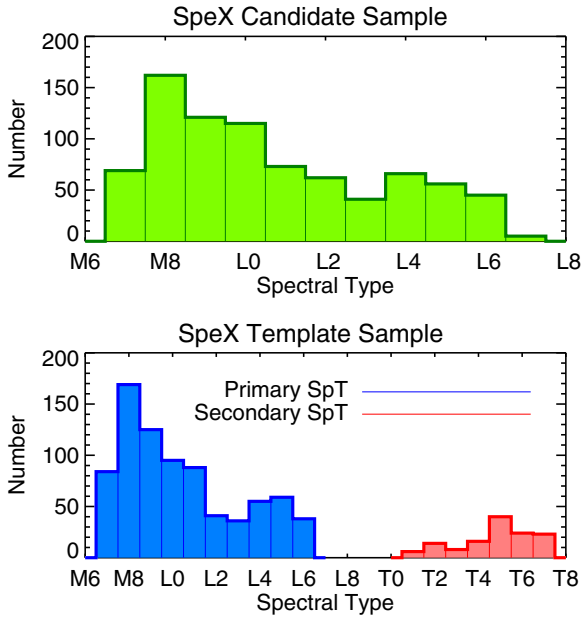

Figure 1. Distribution of SpeX spectral types in the samples used for selecting candidates (top) and template fitting (bottom).

(A color version of this figure is available in the online journal.)

The distribution of spectral types for both samples is shown in Figure 1. In both samples, the number of spectra decreases toward later spectral types owing to declining space densities for L dwarfs (Cruz et al. 2003) and sensitivity limits for late L and T dwarfs. Since there are significantly more sources with late-M spectral types in our samples, it is more likely to find binaries with a late-M primary. The sources included were observed as part of several different programs, including our ongoing program to compile a magnitude-limited sample of L dwarfs (A. Burgasser et al., in preparation). As such, we do not claim the sample to be complete or unbiased.

3. IDENTIFICATION OF SPECTRAL BINARIES

3.1. Visual Inspection

The spectral morphology of unresolved late-M/early-L plus T dwarf binary systems gives rise to a distinctive feature in blended-light spectra: a small "dip" centered at 1.63 μm, which is the combination of CH_4 absorption from the secondary and FeH from the primary (Cushing et al. 2003; Burgasser 2007b). Methane does not exist in the spectra of late-M/early-L dwarfs, so its presence indicates a T dwarf companion. However, this feature is very weak in blended-light spectra since a T dwarf is significantly fainter than the M/L primary (e.g., $\Delta J \sim 3.5$ mag between an M8 and a T5, which is the case for 2MASS J03202839−0446358). Moreover, variations in the spectral slope for a blue or red L dwarf can make this feature ambiguous, as can poor correction of hydrogen lines in the A0V calibrators. Alternative indicators, such as a relatively higher flux around the 1.25 μm peak and an inflated bump shortward of 2.2 μm, may also reveal the presence of a T dwarf companion, or that the spectrum of the source is unusually blue.

To facilitate our visual inspection, we fit the candidate sample to templates of single objects, following the same chi-squared

Table 3
Spectral Indices[a]

Spectral Index	Numerator Range (μm)	Denominator Range (μm)	Feature	Ref.
H_2O-*J*	1.14–1.165	1.26–1.285	1.15 μm H_2O	1
CH_4-*J*	1.315–1.335	1.26–1.285	1.32 μm CH_4	1
H_2O-*H*	1.48–1.52	1.56–1.60	1.40 μm H_2O	1
CH_4-*H*	1.635–1.675	1.56–1.60	1.65 μm CH_4	1
H_2O-*K*	1.975–1.995	2.08–2.10	1.90 μm H_2O	1
CH_4-*K*	2.215–2.255	2.08–2.12	2.20 μm CH_4	1
K/*J*	2.06–2.10	1.25–1.29	$J - K$ color	1
H-dip	1.61–1.64	1.56–1.59 + 1.66–1.69[b]	1.63 μm FeH/CH_4	2
K-slope	2.06–2.10	2.10–2.14	*K*-band shape/CIA H_2	3
J-slope	1.27–1.30	1.30–1.33	1.28 μm flux peak shape	4
J-curve	1.04–1.07 + 1.26–1.29[c]	1.14-1.17	Curvature across *J*-band	4
H-bump	1.54–1.57	1.66–1.69	Slope across *H*-band peak	4
H_2O-*Y*	1.04–1.07	1.14–1.17	1.15 μm H_2O	4

Notes.
[a] Indices were calculated by integrating flux between the specified wavelength ranges.
[b] Denominator is average of these two wavelength ranges.
[c] Numerator is average of these two wavelength ranges.
References. (1) Burgasser et al. 2006a; (2) Burgasser et al. 2010a; (3)Burgasser et al. 2002; (4) this paper.

minimization routine as in Section 3.3, and then subtracted the median combination of the 10 best-fitting single sources from each spectrum. The objects with residuals consistent with a T dwarf spectrum were selected as visual candidates. To validate this procedure, we also performed the same template subtraction on four confirmed spectral binaries: SDSS J000649.16−085246.3, 2MASS J03202839−0446358, SDSS J080531.89+481233.0, and 2MASS J13153094−2649513 (see Table 1). The residuals from these subtractions clearly exhibited T dwarf-like morphologies. Twelve sources were selected as visual candidates.

3.2. Spectral Indices

In addition to visual inspection, we also used spectral indices to identify additional candidate binaries due to the subtlety of T dwarf features in combined-light spectra (Burgasser et al. 2010a). We initially examined standard classification indices from Burgasser et al. (2006a), as well as the "*H*-dip" index from Burgasser et al. (2010a), and further defined five new indices. The new indices were designed by comparing the residuals of the four known binary spectra after subtracting their best single template fits. As a control sample, we also examined single templates subtracted from each other, which showed no evidence for a T dwarf companion.

The new spectral indices specifically designed in this paper are as follows:

1. *H*-bump: measures the peak in the continuum from the T dwarf in the *H* band relative to the dip centered around 1.63 μm seen in M+T binaries, making this index complimentary to *H*-dip. A higher value of *H*-bump implies a larger flux at 1.55 μm, possibly caused by the presence of a T dwarf.
2. *J*-curve: designed to detect the flux coming from both the 1.05 μm and 1.27 μm peaks of a T dwarf, as compared to the deep methane absorption at 1.12 μm.
3. *J*-slope and K_s-slope: measure the slope of the peaks in the *J* and K_s bands at 1.27 μm and 2.10 μm. In both cases, the peaks in a single late-M/early-L should look somewhat flat, giving values close to 1, whereas in a late-M/early-L plus T dwarf binary the slopes of the *J*- and K_s-band peaks are slightly negative and positive, respectively.
4. H_2O-*Y*: measures the prominence of the *Y*-band peak of the T dwarf at ∼1.05 μm compared to the water and methane absorption around ∼1.15 μm. M and L dwarfs do not present peaks in the *Y* band.

The 13 indices examined are described in Table 3. We also used $J - K_s$, $J - H$, and $H - K_s$ colors synthesized from the spectra themselves, and the source spectral type, for a total of 17 parameters.

Comparing all 17 parameters against each other yielded 136 pairings. After visual examination to determine which pairings best segregated the four known M/L+T binaries, 12 combinations were selected (Figure 2). We then used two techniques to define regions of interest in each combination for candidate selection. If a trend among all sources was clear, we fit the points to a second-order polynomial and defined a region demarcated in the *y*-axis by the $+1\sigma$ or -1σ curves from the fit function, and in the *x*-axis by the horizontal spread of the binary benchmarks. Conversely, if the points did not indicate any trends, then the region was demarcated such that it included the four binary benchmarks. The limits to these regions are described in Table 4.

Objects falling in eight or more selection regions were considered strong index candidates, whereas those falling in four to eight regions were considered weak index candidates (Figure 3). The number of selected sources rises steadily below four or five combinations, suggesting that sources selected fewer than four times could be spurious. Three of our benchmarks were selected by all 12 combinations, while SDSS J0006−0852 missed only the SpT/CH_4-H cut, since it falls within one standard deviation from the fitting curve.

In total, 8 strong and 22 weak candidates were selected, including the previously identified spectral binaries 2MASS J20261584−2943124 (Gelino & Burgasser 2010) and 2MASS J13114227+3629235 (Kirkpatrick et al. 2011). Seven visual

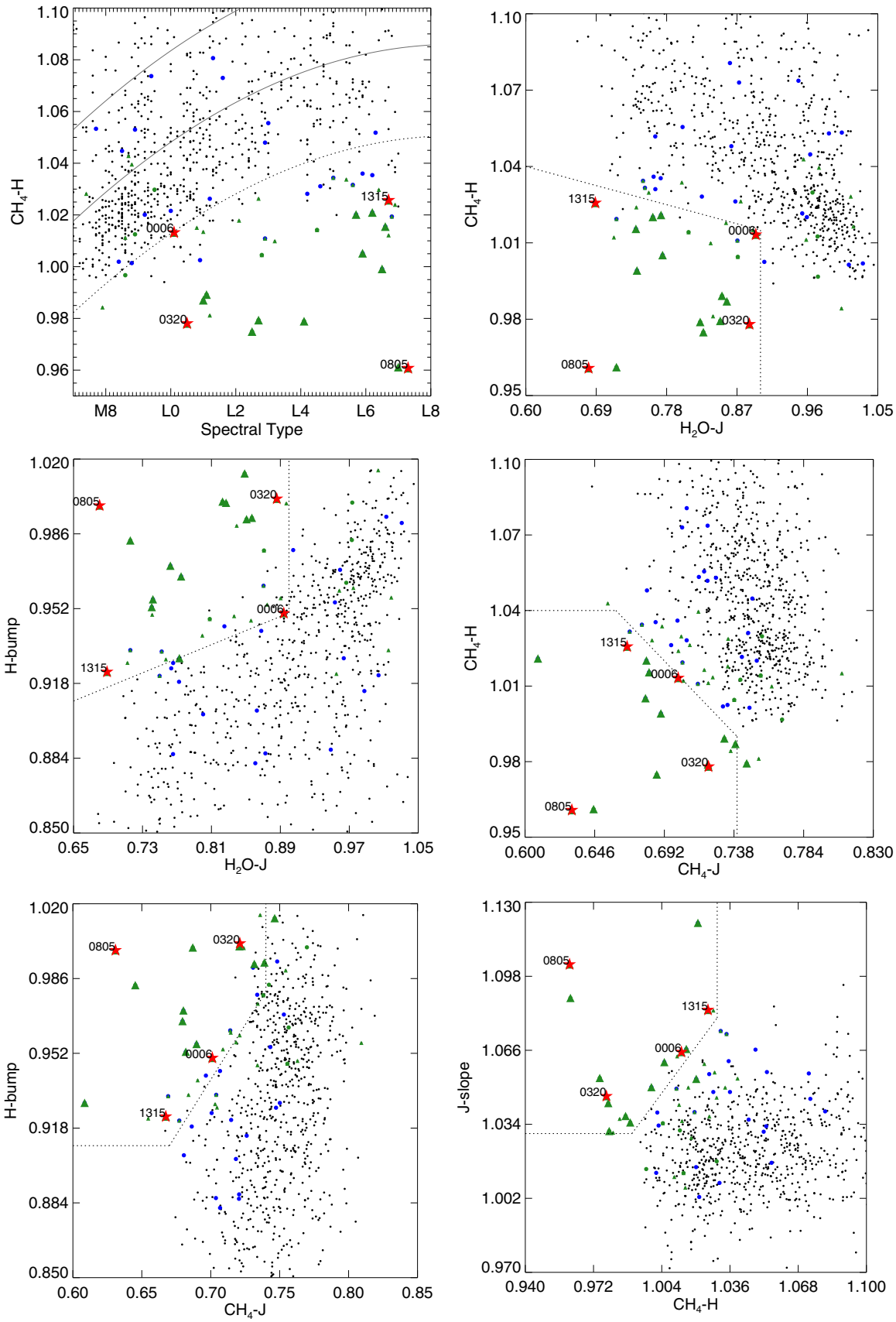

Figure 2. Index selection of spectral binary candidates. The indices calculated from the candidate sample of SpeX spectra are shown in black. The labeled red stars represent the four binary benchmarks. Unusually blue sources are plotted as blue circles, while the large and small green triangles show the strong and weak candidates, respectively. The green circles represent the visual candidates.

(A color version of this figure is available in the online journal.)

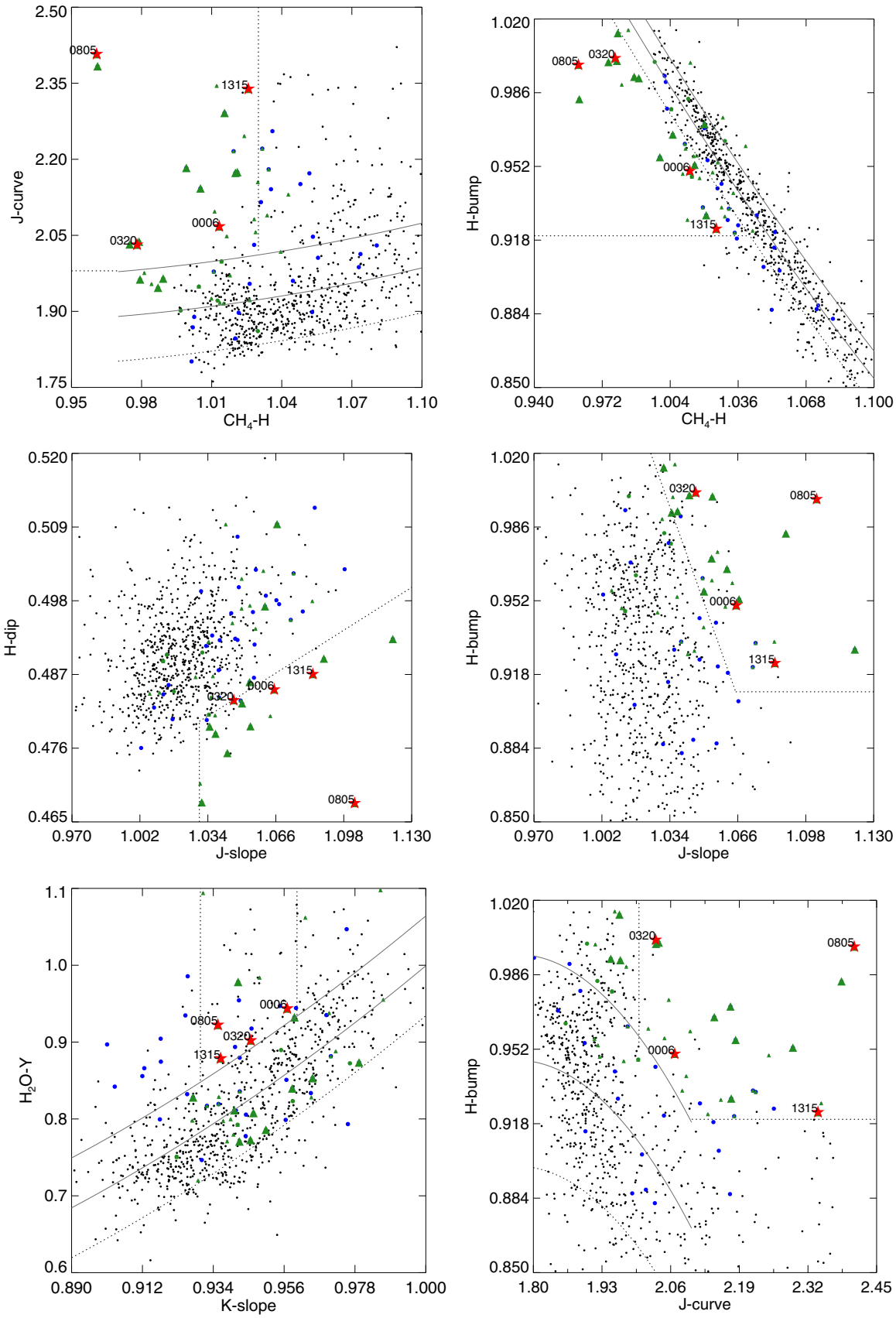

Figure 2. (Continued)

Table 4
Delimiters for selection regions in parameter spaces

x vs. y	Limits
SpT vs. CH_4-*H*	Best fit curve: $y = -4.3 \times 10^{-4}x^2 + 0.0253x + 0.7178$, $\sigma = 0.0354$. Select points below the -1σ curve.
H_2O-*J* vs. CH_4-*H*	Intersection of: $y = -0.08x + 1.09$ and $x = 0.90$. Select points on lower left corner.
H_2O-*J* vs. *H*-bump	Intersection of: $y = 0.16x + 0.806$ and $x = 0.90$. Select points on upper left corner.
CH_4-*J* vs. CH_4-*H*	Intersection of: $y = -0.56x + 1.41$ and $y = 1.04$. Select points on lower left corner.
CH_4-*J* vs. *H*-bump	Intersection of: $y = 1.00x + 0.24$, $x = 0.74$, and $y = 0.91$. Select points on upper left corner.
CH_4-*H* vs. *J*-slope	Intersection of: $y = 1.250x - 0.207$, $x = 1.03$, and $y = 1.03$. Select points on upper left corner.
CH_4-*H* vs. *J*-curve	Best fit curve: $y = 1.245x^2 - 1.565x + 2.224$, $\sigma = 0.088$. Select points above the 1σ curve, up to CH_4-$H = 1.03$.
CH_4-*H* vs. *H*-bump	Best fit curve: $y = 1.36x^2 - 4.26x + 3.89$, $\sigma = 0.013$. Select points below the -1σ curve, down to *H*-bump = 0.92.
J-slope vs. *H*-dip	Intersection of $y = 0.20x + 0.27$ and $x = 1.03$. Select points on lower right corner.
J-slope vs. *H*-bump	Intersection of: $y = -2.75x + 3.84$ and $y = 0.91$. Select points on upper right corner.
K-slope vs. H_2O-*Y*	Best fit curve: $y = 12.036x^2 - 20.000x + 8.973$, $\sigma = 0.064$. Select points above the 1σ curve and between *K*-slope = 0.93-0.96.
J-curve vs. *H*-bump	Best fit curve: $y = 0.269x^2 - 1.326x + 2.479$, $\sigma = 0.048$. Select points above the 1σ and greater than *J*-curve = 2.00 and *H*-bump = 0.92.

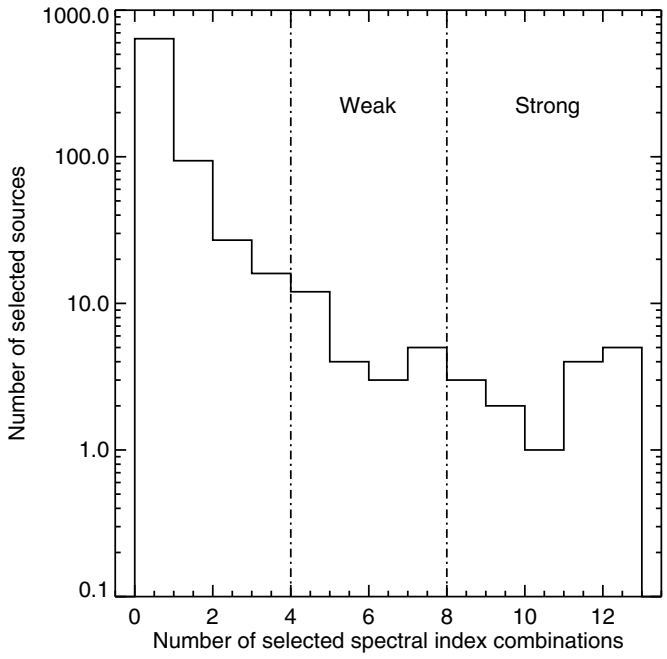

Figure 3. Number of sources satisfying index combinations vs. total number of combinations. Sources selected eight or more times are considered *strong* candidates. Sources selected between four and eight times are considered *weak* candidates.

candidates overlapped with the index candidates: five as strong and two as weak.

3.3. Spectral Template Fitting

To statistically test the binary hypothesis for our visual and index-selected candidates, we compared each spectrum to templates of both single sources and binary systems, using the method described in Burgasser et al. (2010a). The candidates determined by visual inspection or spectral index selection were first rejected from the template pool. Then, all spectra were interpolated onto a common wavelength scale from 0.8 to 2.4 μm and normalized to the peak flux between 1.2 and 1.3 μm. Each candidate spectrum $C[\lambda]$ was directly compared to all single templates $T[\lambda]$ and ranked by a weighted chi-squared statistic:

$$\chi^2 \equiv \sum_{\lambda} w[\lambda] \left[\frac{C[\lambda] - \alpha T[\lambda]}{\sigma_c[\lambda]} \right]^2, \quad (1)$$

where $w[\lambda]$ is a vector of weights proportional to the waveband size of each pixel (see Cushing et al. 2008), α is a scaling factor minimizing χ^2, and $\sigma_c[\lambda]$ is the noise spectrum for each candidate. The statistic was computed over the wavelength ranges $\{\lambda\} = 0.95$–1.35 μm, 1.45–1.80 μm, and 2.00–2.35 μm, avoiding regions of strong telluric absorption.

Binary templates were constructed by first scaling each template spectrum to absolute fluxes using the Two Micron All Sky Survey (2MASS) M_{Ks} versus spectral type relation of Looper et al. (2008a) and then combining all pairs of single templates, such that the spectral type of the primary was earlier than that of the secondary, resulting in a total of 638, 686 binary templates.[14] More specifically, the primary spectral type was fixed to lie between M7 and L7 while the secondary spectral type ranged between T1 and T8, since types earlier than T1 do not evidence strong methane features yet. The best binary fits were ranked using a chi-squared minimization routine. We determined the true significance that a binary template is superior to a single template by comparing the χ^2 distributions of the binary and single fits using the one-sided *F*-test

[14] We do not explicitly include uncertainties for the absolute magnitude to spectral type relation, but the extensive number of binary templates we use already models the intrinsic scatter in the population.

statistic η_{SB}:

$$\eta_{SB} \equiv \frac{\min(\{\chi^2_{single}\})}{\min(\{\chi^2_{binary}\})} \frac{dof_{binary}}{dof_{single}}. \quad (2)$$

Here dof is the degrees of freedom for each fit (Equation (2) in Burgasser et al. 2010a). Candidates with an F-statistic falling under the 90% confidence level were rejected, including five visual candidates. In particular, 2MASS J14493784+2355378 and 2MASS J14232186+6154005 (also a weak index-selected candidate), two previously identified spectral binary candidates from Gizis et al. (2003) and Geißler et al. (2011), were rejected owing to their low confidence level that the binary fit was statistically better than the single fit. Since our template sample includes a wide range of objects such as young and unusually blue and red dwarfs, the peculiarities of these candidates may be better explained by factors other than unresolved binarity. One exception to the index selection was 2MASSI J1711457+223204, whose SpeX spectral type was too late to be included in the candidate sample, yet it was a visual candidate and passed the binary fit F-test. Figures 4 and 5 show the best single (left) and binary (right) template fits to our strong and weak candidates. Table 5 summarizes the results of these fits.

Upon further visual examination, some binary fits still proved unsatisfactory. This was the case for the blue L dwarfs 2MASS J11181292−0856106, 2MASS J14162409+1348267, 2MASS J15150083+4847416, and 2MASS J17114558+40285779 and the subdwarfs 2MASS J03303847−2348463, 2MASS J03301720+3505001, 2MASS J04024315+1730136, 2MASS J15412408+5425598, and 2MASS J23311807+4607310. Section 5.1 discusses these issues in more detail. As a result, 14 candidates have been recognized, of which 11 are newly identified.

In an effort to balance the trade-off between fidelity of binary candidates and completeness, we are leaning toward the former. Our binary selection criteria are conservative, and it is likely that other spectral binaries may be identified with slightly looser constraints.

4. INDIVIDUAL CANDIDATES

In summary, from the ∼800 sources compiled in the candidate sample, 12 were selected by visual inspection and 30 were selected by spectral indices. Seven sources overlapped the results of these selection methods. After fitting all 35 candidates, 17 were rejected owing to their confidence level being lower than 90%, and four more owing to their unusually blue colors (see Section 5.1), leading to a final count of 14: 6 strong, 7 weak, and 1 visual candidate not overlapping with the index selected. Labels of strong and weak candidates come from index selection.

4.1. Strong Candidates

4.1.1. 2MASS J02361794+0048548

Originally discovered by Geballe et al. (2002), 2MASS J0236+0048 was classified as an L6 in the optical and L6.5 in the infrared by Casewell et al. (2008). In their study, Casewell et al. (2008) comment that this object may belong to the Pleiades moving group, given its proper motion of $[\mu_\alpha \cos\delta, \mu_\delta] = [161.33 \pm 10.10, 176.33 \pm 19.16]$ mas yr^{-1} and agreement between photometric and moving group distances at $d = 26$ pc. However, Scholz et al. (2009) reclassified this object as an L9, reducing its spectroscopic distance to 18 pc, while its strong FeH band at 0.99 μm argues against low surface gravity (Allers et al. 2007). Nevertheless, the spectrum of this source does not show any signs of youth (Allers et al. 2007). 2MASS J0236+0048 is selected by 11 out of 12 spectral index combinations, and its binary fit is significantly better than its single fit, making this a strong binary candidate with L5.0 ± 0.6 and T1.9 ± 1.1 components.

4.1.2. SDSS J093113.09+280228.9

Schmidt et al. (2010) discovered SDSS J0931+2802 in the SDSS catalog and classified it as an L3 at a mean distance of 29 ± 9 pc. Its spectrum shows excess flux in the J band at ∼1.27μm and a noticeable dip in the H band in the vicinity of 1.63 μm, as expected for a T dwarf component. This source was selected as a visual candidate, and by 11 out of 12 spectral index combinations, and our spectral fitting predicts component types of L1.4 ± 0.1 and T2.6 ± 0.9.

4.1.3. 2MASS J13114227+3629235

Identified as a brown dwarf candidate by Zhang et al. (2009), 2MASS J1311+3629 is a peculiar L5. While also classified as unusually blue in wavelengths longer than J band (Mace et al. 2013), it lacks evidence of low metallicity or H_2 collision-induced absorption (CIA) in H and K bands. Kirkpatrick et al. (2011) identified the methane feature in the H band centered around 1.63 μm, suggesting unresolved binarity. In this study, it was selected by 11 spectral index combinations and also as a visual candidate owing to its methane absorption band starting at 1.60 μm. Template fitting gives spectral types of L4.8 ± 0.6 and T4.1 ± 2.7.

4.1.4. 2MASS J13411160−30525049

2MASS J1341−3052 was discovered by Reid et al. (2008) and classified as an L3 in the optical by Faherty et al. (2009), who also measured its parallax and distance (24±2 pc). 2MASS J1341−3052 was selected by eight spectral indices, and its spectral fitting suggests component spectral types of L1.2 ± 0.3 and T6.3 ± 1.0.

4.1.5. 2MASS J14532589+1420418

2MASS J1453+1420 was classified as an L1 in both the infrared (Kirkpatrick et al. 2010) and the optical (Schmidt et al. 2010), where it clearly shows excess flux in the J band and a dip in the H band. It is selected by 11 out of 12 spectral index combinations, and it is slightly blue with a $J - K_s$ color of 1.18 ± 0.05 as compared to the median for the L1 spectral type 1.34 ± 0.19 (Schmidt et al. 2010). It is best fit by L1.1 ± 0.0 and T6.0 ± 1.1 components.

4.1.6. 2MASS J20261584−2943124

2MASS J2026−2943 had already been identified as a spectral binary candidate by Gelino & Burgasser (2010), but it failed to be resolved by Keck AO, thus setting an upper limit in separation of 0.″25 or a projected separation of 9 AU at a distance of 36 ± 5 pc (Gelino & Burgasser 2010). This source clearly shows a dip in its spectrum centered at 1.63 μm, and it is best fit by a combination of L1.0 ± 0.5 and T5.8 ± 1.0 components.

4.2. Weak Candidates

4.2.1. 2MASS J02060879+22355930

2MASS J0206+2235 was discovered and classified as an L5.5 by Chiu et al. (2006), and characterized as a blue L dwarf by

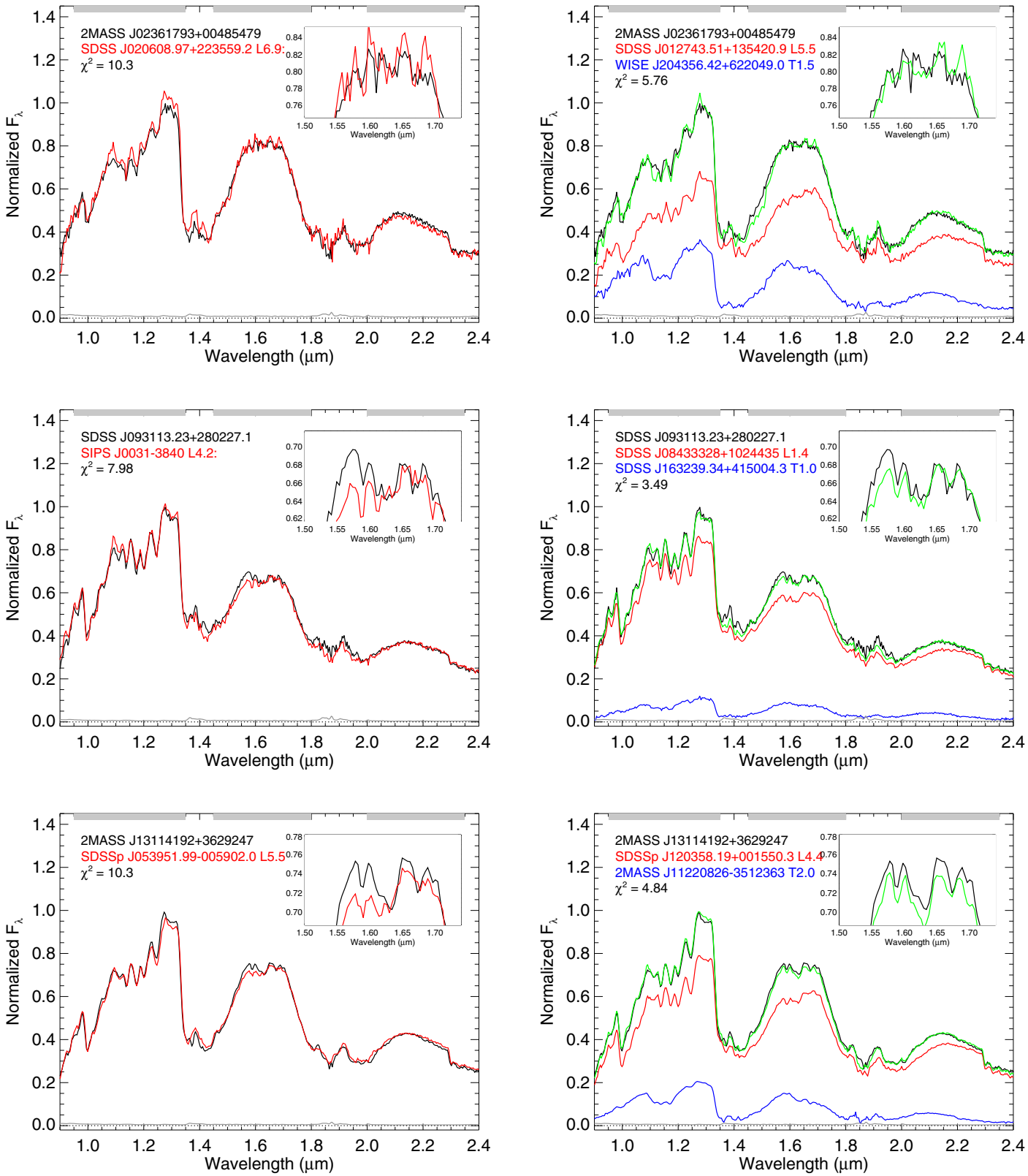

Figure 4. Best fits to single (left) and binary (right) templates for our strong candidates. The black line shows the candidate spectrum. For the single fits, the red line is the best single template. For the binary fits, the green line is the best binary template, which is the addition of the red (primary) and blue (secondary) lines. The gray line represents the uncertainty in the candidate spectrum. The gray horizontal bars at the top of the figures mark the parts of the spectrum being fit, while water absorption dominates the gaps. Notice the significant fitting improvement on the binary fits as compared to the single fits, particularly around the methane absorption feature centered at 1.63 μm (see inset).

(A color version of this figure is available in the online journal.)

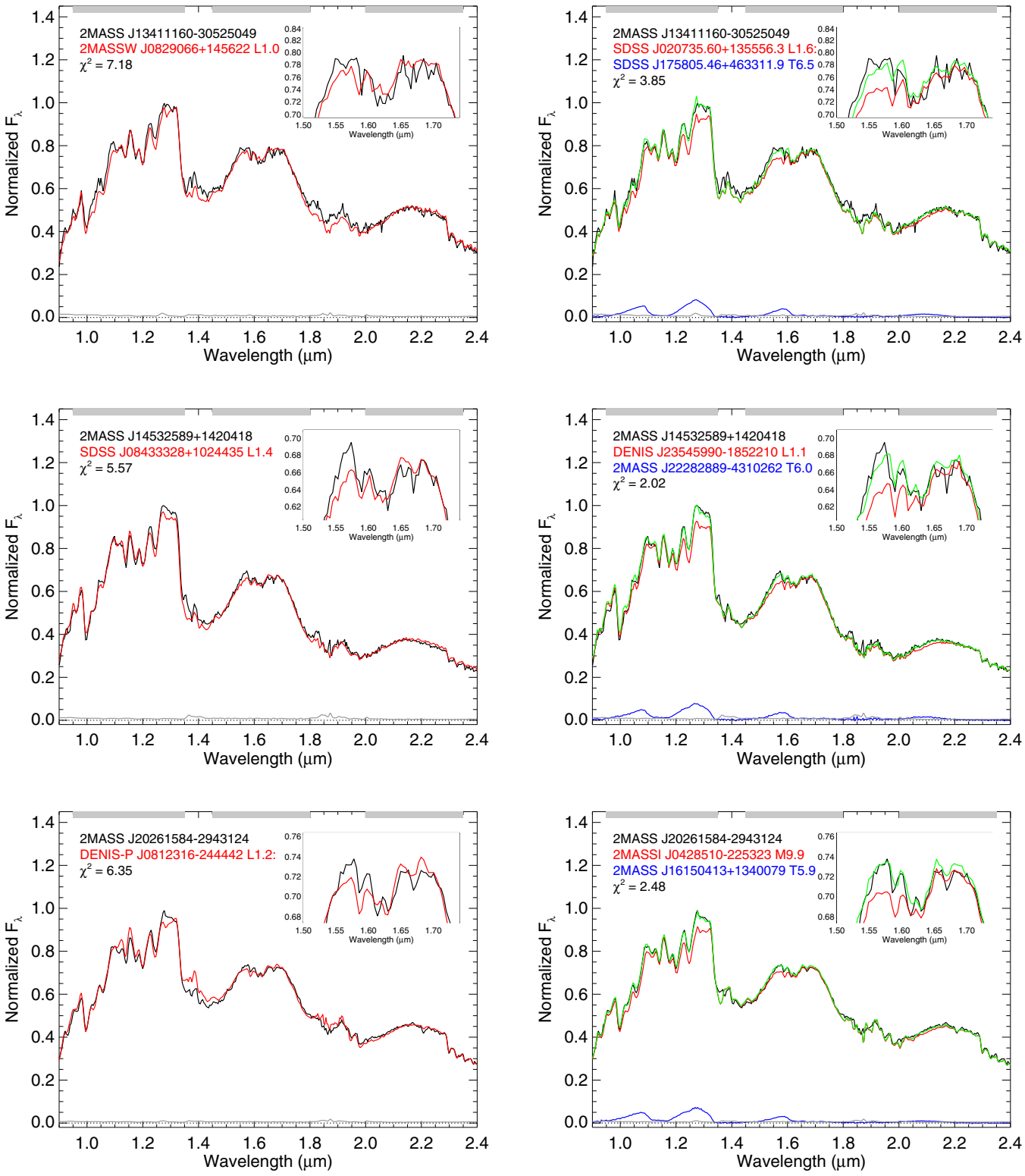

Figure 4. (Continued)

Schneider et al. (2014). It was selected by seven spectral index combinations and fit to L5.1 ± 0.5 and T3.2 ± 2.3 components.

4.2.2. DENIS-P J04272708−1127143

2MASS J0427−1127 was discovered and classified as an M7 by Martín et al. (2010). It was selected by five spectral index combinations and best fit by M7.4 ± 0.2 and T5.1 ± 1.5 components.

4.2.3. 2MASS J10365305−3441380

2MASS J1036−3441 was classified as an L6 (Gizis 2002) at a distance of 21 ± 3 pc. It almost made the cut for a strong candidate, since it was selected by seven spectral index combinations. This source was best fit by components with L5.2 ± 0.4 and T1.4 ± 0.4 spectral types. Despite not having a pronounced methane absorption feature centered at 1.63 μm, the binary fit

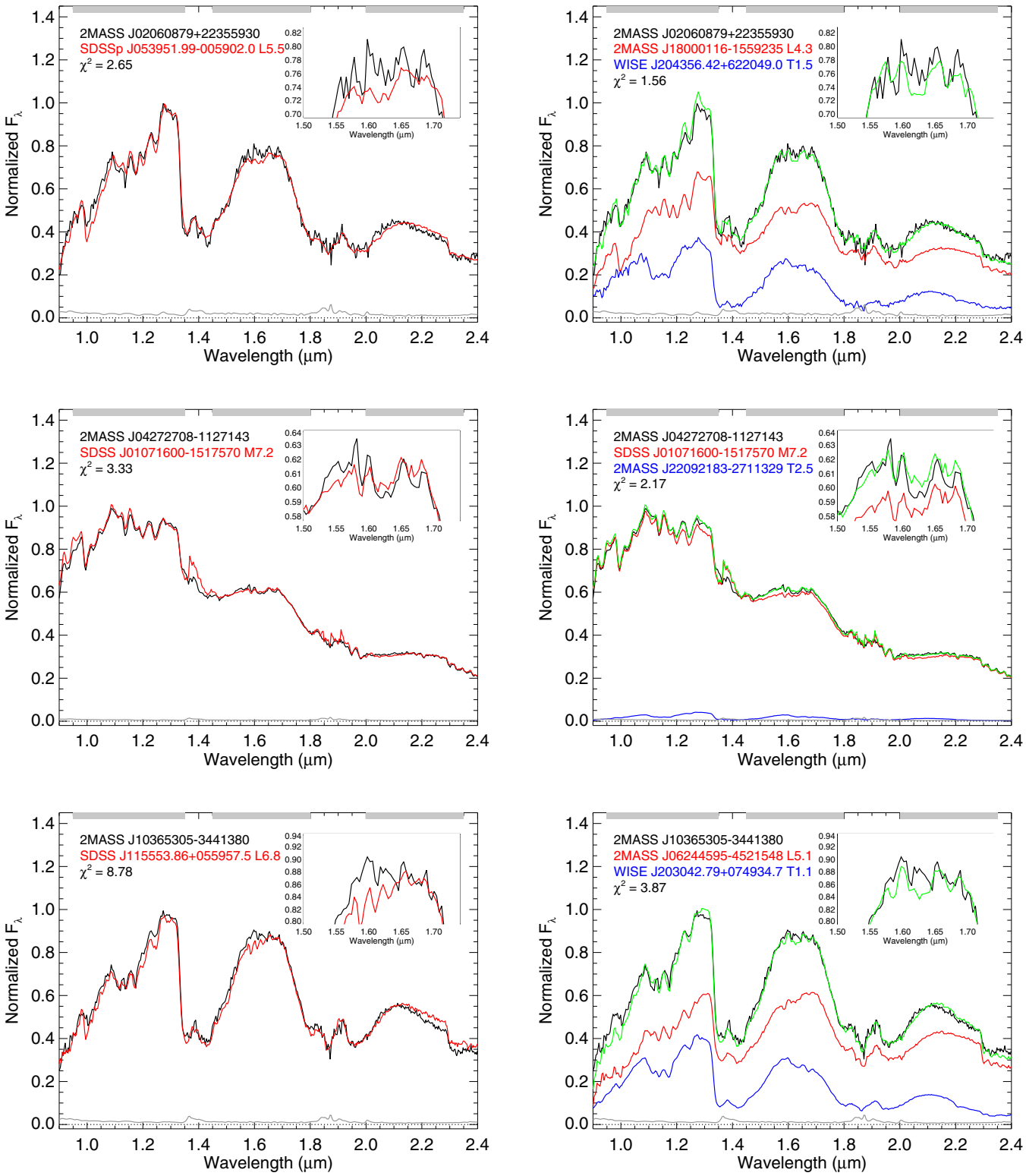

Figure 5. Best fits to single (left) and binary (right) templates for our weak candidates. Same color code as for Figure 4.
(A color version of this figure is available in the online journal.)

is significantly better than the single fit, especially at the *J*-band peak.

4.2.4. 2MASS J10595138−2113082

2MASS J1059−2113 is an L1 (Cruz et al. 2003) at a distance of 32.1 ± 2.2 pc. This source was selected by four spectral index combinations, and its best binary fit yields components with L0.6 ± 0.4 and T3.4 ± 1.3 spectral types. Its spectrum shows a strong absorption feature centered at 1.63 μm, as well as a flux excess at 1.23 μm and 2.20 μm.

4.2.5. SDSS J142227.20+221557.5

SDSS J1422+2215 was identified and classified as an L6 in the NIR by Chiu et al. (2006) and also as an unusually blue

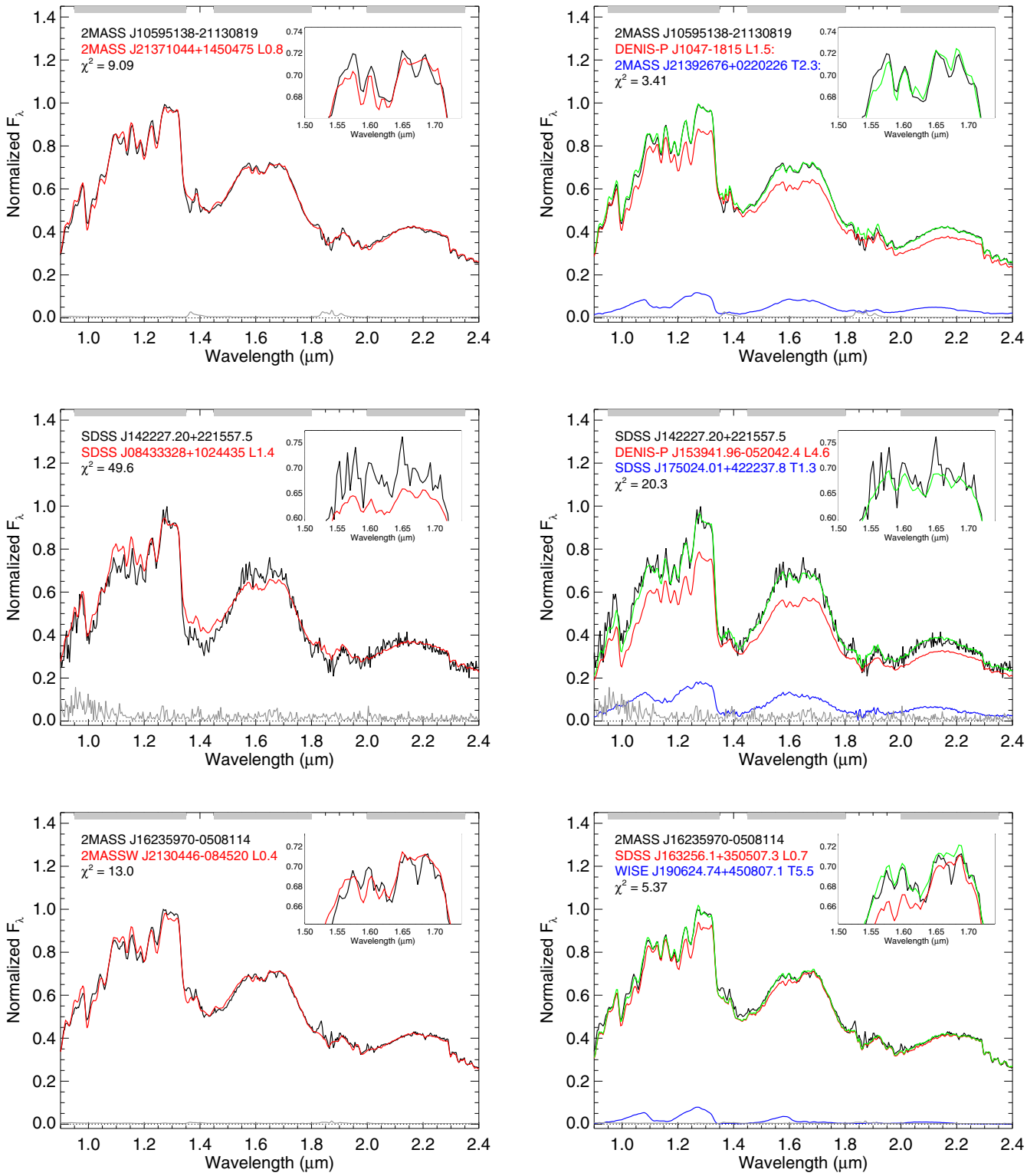

Figure 5. (Continued)

L dwarf, showing strong H_2O and FeH absorption bands, which may be due to subsolar metallicity and/or thinner condensate cloud decks. It was selected by 4 out of 12 spectral index combinations with most likely component spectral types of L4.2 ± 0.6 and T4.1 ± 2.3.

4.2.6. WISE J16235970−0508114

WISE J1623−0508 was classified as an L1 in the NIR (Thompson et al. 2013). This source was selected by four spectral index combinations and best fit by L0.6 ± 0.3 and T6.0 ± 0.3 components.

4.2.7. 2MASS J17072529−0138093

2MASS J1707−0138 was discovered and classified as an L2 by Martín et al. (2010). Selected by five spectral index combinations, its spectrum is best fit by components with L0.7 ± 0.5 and T4.3 ± 2.0 spectral types. Its spectrum shows a strong absorption feature centered at 1.63 μm.

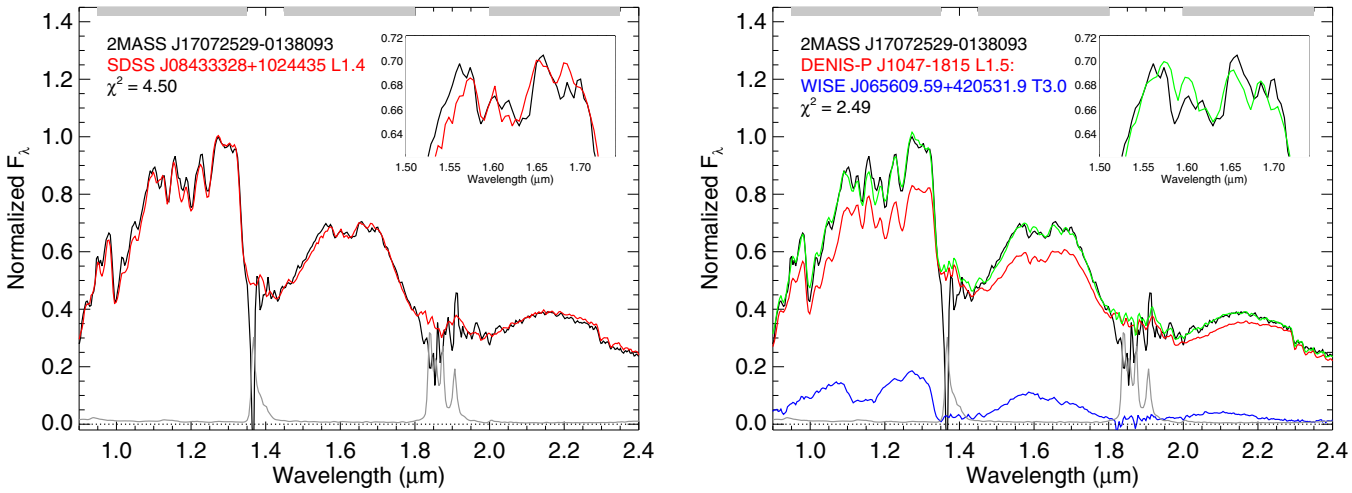

Figure 5. (Continued)

4.3. Visual Candidates

4.3.1. 2MASSI J1711457+223204

2MASS J1711+2232 was first identified and classified as an L6.5 in the optical by Kirkpatrick et al. (2000). Owing to its FeH and CH_4 absorption features in the *H* band, Burgasser et al. (2010a) suggested that it could be a spectral binary with L5.0 and T5.5 components. We find slightly different component spectral types of L1.5 ± 0.6 and T2.5 ± 1.0, yet this source was not selected by spectral indices because of its late SpeX spectral type of L8.8. Despite having been imaged with *HST*/WFPC, it remains unresolved (Gizis et al. 2003).

5. DISCUSSION

5.1. Blue L Dwarfs as Contaminants

Four of the candidates selected by spectral indices were rejected after spectral fitting owing to their poor binary fits. An example is shown in Figure 7. When we investigated these sources in detail, we found they were classified as blue objects in the literature and/or showed an unusually blue spectrum. 2MASS J11181292−0856106 was classified as a metal-poor subdwarf by Kirkpatrick et al. (2010). SDSS J141624.09+134826.7 is part of a resolved binary system with a T7.5 companion (Burningham et al. 2010; Burgasser et al. 2010b; Scholz 2010) that is itself a blue outlier. Bowler et al. (2010) rejected unresolved binarity for the primary based on a qualitative comparison to the unusually blue L dwarf 2MASS J11263991−5003550. The L6 2MASS J15150083+4847416 shows a stable RV of -29.97 ± 0.14 km s^{-1} (Wilson et al. 2003) and no signs of binarity from its spectrum. Finally, 2MASS J17114558+40285779 was discovered by Radigan et al. (2008) as an unusually blue wide companion to the K star G203-50. They discuss the possibility that the object may be unusual owing to unresolved binarity, but they argue in favor of low metallicity. For all of these sources, the lack of single templates akin to blue objects resulted in statistically better binary fits, yet the match is still relatively poor around the 1.63 μm methane absorption feature.

A few more previously unidentified NIR subdwarfs were also selected as weak candidates and subsequently rejected owing to their poor binary fits. The best binary fits for 2MASS J03303847−2348463, 2MASS J03301720+3505001, 2MASS J04024315+1730136, 2MASS J15412408+5425598, and 2MASS J23311807+4607310 use another subdwarf as a primary, which again indicates that they are part of a rare blue population that has a short supply of examples in this sample.

M+T binaries have slightly bluer spectra caused by the extra flux in the *J* band corresponding to the peak in the T dwarfs. Particularly, some sources originally classified as unusually blue have been later identified as spectral binaries (e.g., SDSS J0805+4812; Burgasser 2007b; Dupuy & Liu 2012). In contrast, intrinsically blue L dwarfs have low metallicity, thin cloud coverage, large-grain clouds, or a combination of these, causing a blue tilt to the NIR spectrum (Schmidt et al. 2010; Burgasser et al. 2008b; Cruz et al. 2007). Faherty et al. (2009) have defined red and blue photometric outliers as the objects whose $J - K_s$ color placed them 2σ or 0.4 mag away from the average for their spectral type, while pointing out the difficulty to distinguish outliers beyond a spectral type of L9 due to the small sample of objects. Figure 8 shows the $J - K$ colors for our sample as compared to their spectral types, including the median and $\pm 2\sigma$ lines as calculated from the sample (solid lines) and reported in the literature (dashed lines) by West et al. (2011) and Schmidt et al. (2010) for samples of M and L dwarfs, respectively. Figure 8 suggests that blue L dwarfs are a major contaminant in our sample since a significant fraction of both known binaries and candidates have similar colors and thus lie in the same region as blue sources. We conclude that the blue L dwarf contaminants can be recognized if rejected as a result of their poor fits to binary template spectra.

5.2. Separation Distribution of Binary Systems

True confirmation of our candidates requires observational follow-up to either resolve the systems or measure RV or astrometric variability. As noted in the introduction, spectral binaries can be used to devise an unbiased method to measure the VLM binary separation distribution. Therefore, it is worth examining the separation distribution of VLM and brown dwarf spectral binaries confirmed to date, to see whether there are any differences compared to the resolved population.

Figure 9 shows the distribution of projected separations from 122 confirmed VLM binaries.[15] Among the observational

[15] Based on the compilation at the Very-Low-Mass Binaries Archive, http://www.vlmbinaries.org, and more recent discoveries by Choi et al. (2013), Duchêne et al. (2013), Luhman (2013), Radigan et al. (2013), Sahlmann et al. (2013), Burgasser et al. (2012), Liu et al. (2012), Artigau et al. (2011), Burgasser et al. (2011b), Dhital et al. (2011), Gelino et al. (2011), Geißler et al.

Table 5
Binary Candidates Resulting from Spectral Fitting

Source	Primary SpT[a]	Secondary SpT[a]	Confidence[b]	ΔJ	ΔK	SB Ref.	Comments[c]
			Strong candidates				
2MASS J02361794+0048548	L5.0 ± 0.6	T1.9 ± 1.1	97%	1.05 ± 0.48	1.80 ± 0.55	1	···
SDSS J093113.23+280227.1	L1.4 ± 0.1	T2.6 ± 0.9	>99%	2.22 ± 0.23	2.74 ± 0.25	1	V, B
2MASS J13114227+3629235	L4.8 ± 0.6	T4.1 ± 2.7	>99%	2.19 ± 1.02	3.14 ± 1.33	5	V
2MASS J13411160-30525049	L1.2 ± 0.3	T6.3 ± 1.0	98%	3.28 ± 0.53	4.82 ± 0.63	1	V
2MASS J14532589+1420418	L1.1 ± 0.0	T6.0 ± 1.1	>99%	3.27 ± 0.46	4.42 ± 0.63	1	V, (B)
2MASS J20261584-2943124	L0.1 ± 0.5	T5.8 ± 1.0	>99%	3.42 ± 0.40	4.82 ± 0.57	4	V
			Weak candidates				
2MASS J02060879+22355930	L5.1 ± 0.5	T3.2 ± 2.3	95%	1.61 ± 0.89	2.36 ± 1.25	1	···
DENIS-P J04272708-1127143	M7.4 ± 0.2	T5.1 ± 1.5	92%	4.13 ± 0.62	4.98 ± 0.84	1	···
2MASS J10365305-3441380	L5.2 ± 0.4	T1.4 ± 0.4	>99%	0.51 ± 0.32	1.41 ± 0.24	1	···
2MASS J10595138-2113082	L0.6 ± 0.4	T3.4 ± 1.3	>99%	2.58 ± 0.32	3.30 ± 0.64	1	V
SDSS J142227.20+221557.5	L4.2 ± 0.6	T4.1 ± 2.3	96%	2.36 ± 0.78	3.22 ± 1.18	1	B
WISE J16235970-0508114	L0.6 ± 0.3	T6.0 ± 0.8	>99%	3.39 ± 0.40	4.80 ± 0.53	1	···
2MASS J17072529-0138093	L0.7 ± 0.5	T4.3 ± 2.0	97%	2.87 ± 0.75	3.75 ± 1.01	1	···
			Visual candidates				
2MASSI J1711457+223204	L1.5 ± 0.6	T2.5 ± 1.0	>99%	1.20 ± 0.40	3.08 ± 0.64	6	V
			Rejected blue L dwarfs[d]				
2MASS J11181292-0856106	L1.4 ± 0.7	T2.3 ± 2.3	93%	1.50 ± 0.82	2.42 ± 1.11	···	B
SDSS J141624.09+134826.7	L4.4 ± 1.1	T3.9 ± 1.4	>99%	2.12 ± 0.42	2.99 ± 0.67	···	B
2MASS J15150083+4847416	L5.0 ± 0.6	T2.7 ± 1.9	93%	1.32 ± 0.61	2.17 ± 0.84	1	B
2MASS J17114559+4028578	L4.4 ± 0.3	T2.7 ± 0.8	>99%	1.60 ± 0.18	2.32 ± 0.33	···	B
			Rejected candidates				
2MASS J03205965+1854233	M7.8 ± 0.1	T6.0 ± 1.5	58%	4.43 ± 0.73	5.47 ± 0.92	···	V
2MASS J03264453+1919309	M8.5 ± 0.0	T6.7 ± 0.8	87%	4.66 ± 0.50	5.91 ± 0.58	···	V
2MASS J03303847-2348463	M7.7 ± 0.3	T5.6 ± 1.6	49%	3.97 ± 0.85	4.58 ± 1.05	···	···
2MASS J03301720+3505001	M7.7 ± 0.5	T5.3 ± 1.7	55%	4.27 ± 0.81	5.08 ± 1.03	···	···
2MASS J03440891+0111249	L0.6 ± 0.5	T4.8 ± 2.1	56%	3.34 ± 0.88	4.14 ± 1.19	···	···
2MASS J04024315+1730136	M7.5 ± 0.2	T5.4 ± 1.7	48%	4.59 ± 0.78	5.29 ± 1.01	···	···
2MASS J04430581-3202090	L4.5 ± 0.3	T1.7 ± 1.0	85%	1.41 ± 0.34	2.05 ± 0.39	1	B
2MASS J08433328+1024435	L0.9 ± 0.3	T4.9 ± 2.0	80%	3.01 ± 0.75	3.99 ± 1.03	···	···
2MASS J08475148+0138110	L2.0 ± 0.7	T5.7 ± 2.1	59%	3.19 ± 0.74	4.61 ± 1.07	···	···
2MASS J14232186+6154005	L1.9 ± 0.8	T4.6 ± 1.9	72%	2.63 ± 0.67	3.78 ± 0.97	3	V
2MASS J14493784+2355378	M9.4 ± 0.3	T6.2 ± 1.7	51%	4.22 ± 0.69	5.39 ± 1.00	2	V
2MASS J15412408+5425598	M7.6 ± 0.3	T5.4 ± 1.6	55%	4.53 ± 0.75	5.22 ± 0.99	···	···
2MASS J16403561+2922225	M8.1 ± 0.7	T5.3 ± 1.7	51%	4.38 ± 0.77	5.09 ± 1.00	···	···
2MASS J17175402+64274503	M8.5 ± 0.1	T4.6 ± 1.8	86%	4.18 ± 0.70	4.93 ± 1.02	···	···
2MASS J19064847+4011068	L0.0 ± 0.4	T5.9 ± 1.8	74%	3.68 ± 0.75	4.85 ± 1.01	···	···
2MASS J20472471+1421526	M8.4 ± 0.2	T5.7 ± 1.6	81%	4.10 ± 0.70	5.13 ± 0.95	···	V
2MASS J23311807+4607310	M7.5 ± 0.0	T5.7 ± 1.5	53%	4.60 ± 0.75	5.30 ± 0.95	···	···

Notes.
[a] Uncertainties include systematics from spectral classification of Burgasser (2007a).
[b] Confidence that the source fits the binary template better than the single template based on a one-sided *F*-test. See Section 3.3.
[c] B, unusually blue L dwarf; (B), from this paper; V, also a visual candidate.
[d] See Section 5.1.
References. (1) this paper; (2) Bouy et al. 2003; (3) Geißler et al. 2011; (4) Gelino & Burgasser 2010; (5) Kirkpatrick et al. 2011; (6) Burgasser et al. 2010a.

methods for detecting binaries, such as direct imaging, RV variations, astrometric variations, and microlensing, direct imaging has proven to be the most successful so far (73% of confirmed VLM binaries), but its biggest drawback is its limit in resolution. At minimum angular scales of 0.″1–0.″2 for AO and *HST* programs, and typical distances of field brown dwarfs of 20–30 pc, telescope sensitivity reaches its limit at separations of around 2–6 AU. At 2.90 AU, the mean projected separation of eight independently confirmed spectral binaries plotted in Figure 9 falls at the lower end of this sensitivity limit, at less than the mean of known VLM binaries excluding the spectral binaries (3.75 AU), raising the possibility that there may be significantly more tightly bound systems.

To assess whether this is a significant difference, we performed a two-sample Kolmogorov–Smirnov test comparing the projected separation distributions of all binary systems to the confirmed spectral binaries. Specifically, the distributions were constrained in angular separation to 50–500 mas, where the lower limit corresponds to the smallest possible imaging resolution in good seeing, while the upper limit restricts the

(2011), Liu et al. (2011), Allers et al. (2010), Burgasser et al. (2010a), Hwang et al. (2010), Stumpf et al. (2010), Allers et al. (2009) and Luhman et al. (2009).

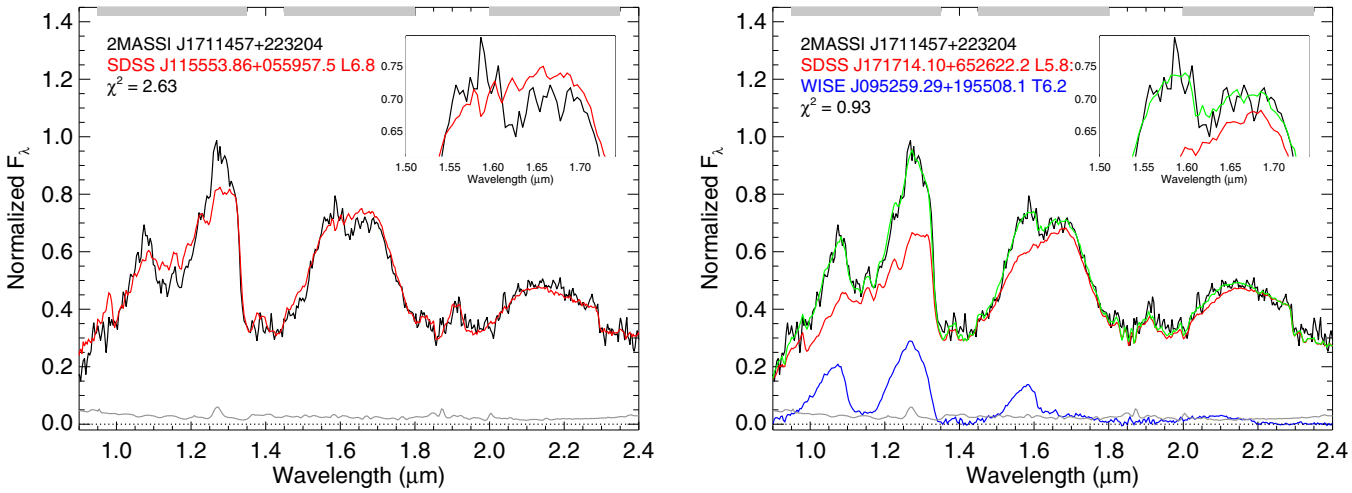

Figure 6. Best fits to single (left) and binary (right) templates for the only visual candidate not selected by indices. Same color code as for Figure 4.
(A color version of this figure is available in the online journal.)

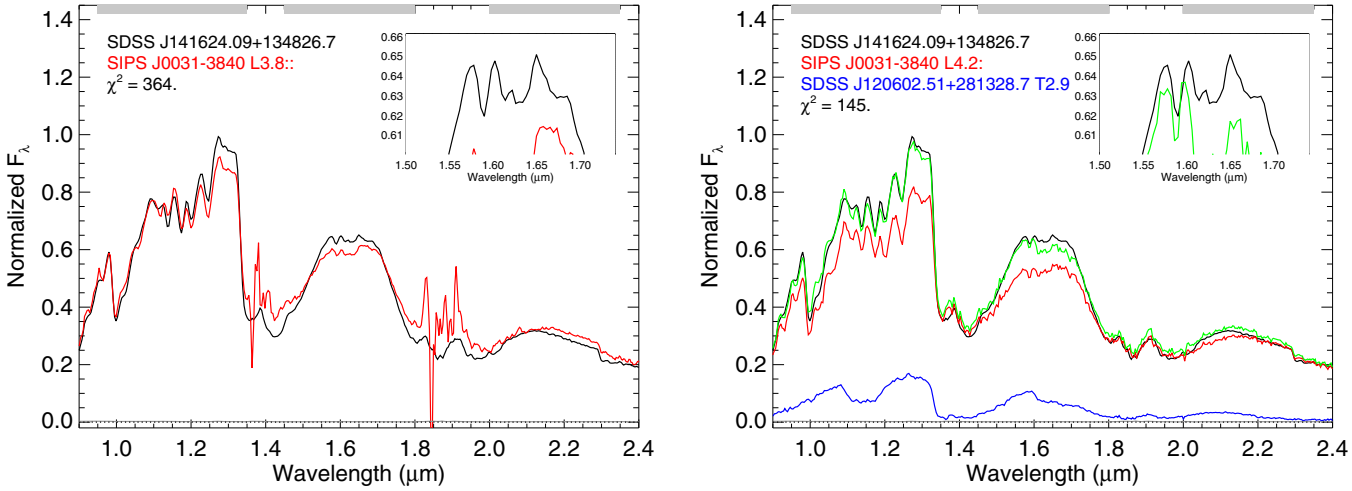

Figure 7. Example of best fits to the blue L dwarf SDSS J141624.09+134826.7.
(A color version of this figure is available in the online journal.)

maximum size of the slit. In addition, the distance was constrained to less than 30 pc, since objects that are farther away would be more difficult to confirm as binaries. In this way, we intend to fairly compare the spectral binary method to the other available methods for binary detection. These constraints reduced the number of spectral binaries to six. The result was a D statistic of 0.41 and a probability of 25%. While the low probability is indicative of a difference between the samples, the small sample size makes this statistic inconclusive. Many more of the existing spectral binaries need to be characterized before a significant difference can be confirmed or ruled out.

6. SUMMARY

We have identified 14 brown dwarf binary candidates with late-M/early-L plus T dwarf components based on visual inspection of low-resolution data and analysis with spectral indices and template fitting. We combined five new spectral indices, with previously defined ones, spectral type, and $J - H$, $H - K_s$, and $J - K_s$ colors to define pairings that effectively select spectral binary candidates, and we confirmed them by comparison to both single and binary template spectra from the SpeX Prism Library. Unusually blue L dwarfs were the main contaminant of this analysis, with four candidates classified as unusually blue but nonetheless being poorly matched to binary spectra. Exploring the separation distribution of binary systems, we find suggestive evidence that spectral binaries are more closely separated than other binaries, but the confirmed sample is too small to be conclusive. We are now undertaking follow-up AO imaging and RV monitoring of these candidates to confirm them and measure orbital properties.

The authors thank telescope operators for their assistance during the observations. D.B.G. would like to thank the Friends of the International Center at UCSD for their generous scholarship, as well as Davy Kirkpatrick and fellow graduate students Alex Mendez and David Vidmar for their helpful discussion and coding tips. This publication makes use of data from the SpeX Prism Spectral Libraries, maintained by Adam Burgasser at http://www.browndwarfs.org/spexprism, the Dwarf Archives Compendium, maintained by Chris Gelino at http://DwarfArchives.org, and the VLM Binaries Archive, maintained by Nick Siegler at http://vlmbinaries.org. The authors wish to recognize and acknowledge the very significant

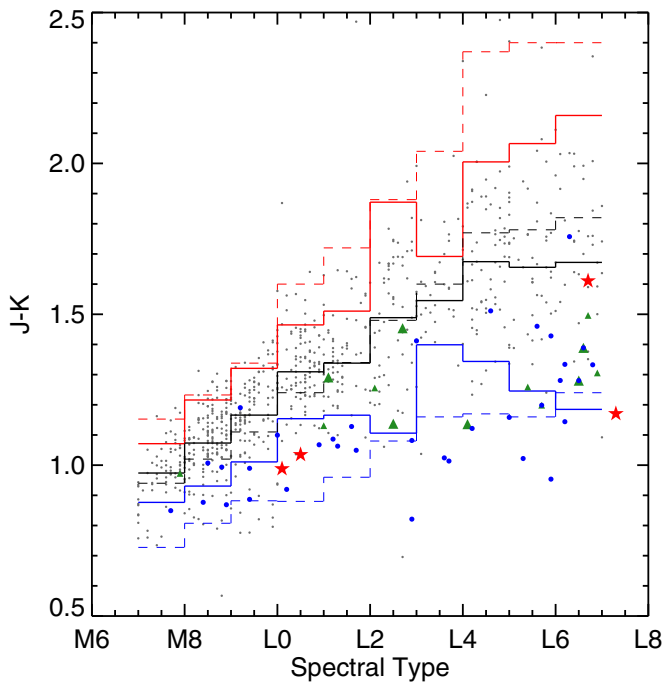

Figure 8. Comparison of spectrophotometric $J - K_s$ colors of the "candidate" sample as a function of spectral type. The solid black line shows the median $J - K$ colors from the sample, while the dashed black line represents the median $J - K$ colors as calculated by West et al. (2011) and Schmidt et al. (2010) from samples of M and L dwarfs. The $+2\sigma$ and -2σ boundaries are indicated in red and blue, respectively. The dashed lines indicate the $+2\sigma$ and -2σ boundaries from West et al. (2011) and Schmidt et al. (2010). Outliers to these regions indicate unusually red and blue dwarfs as described by Faherty et al. (2009). Red stars indicate confirmed M/L+T binaries, while large and small green triangles are strong and weak binary candidates as selected by spectral indices. Blue circles represent unusually blue sources as listed in the literature.

(A color version of this figure is available in the online journal.)

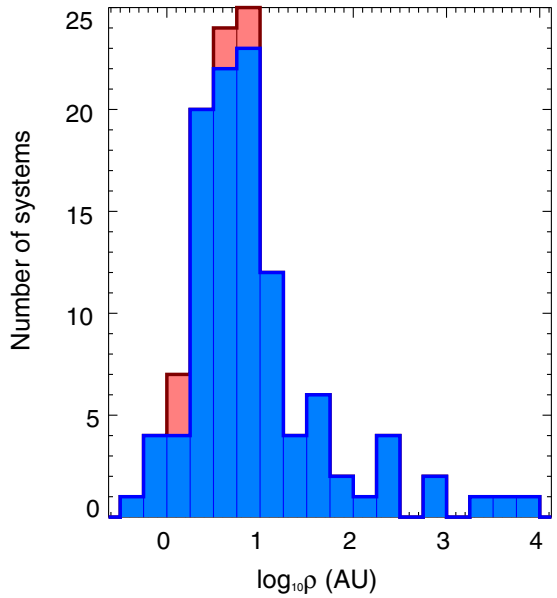

Figure 9. Projected separation (ρ) distribution of 122 confirmed brown dwarf and VLM binary systems from the Very Low Mass Binaries Archive. Spectral binaries are shown in red. Binary systems with only upper limits in separation have been excluded.

(A color version of this figure is available in the online journal.)

cultural role and reverence that the summit of Mauna Kea has always had within the indigenous Hawaiian community. We are most fortunate to have the opportunity to conduct observations from this mountain.

Facility: IRTF (SpeX)

REFERENCES

Allen, P. R. 2007, ApJ, 668, 492
Allers, K. N., Jaffe, D. T., Luhman, K. L., et al. 2007, ApJ, 657, 511
Allers, K. N., & Liu, M. C. 2013, ApJ, 772, 79
Allers, K. N., Liu, M. C., Dupuy, T. J., & Cushing, M. C. 2010, ApJ, 715, 561
Allers, K. N., Liu, M. C., Shkolnik, E., et al. 2009, ApJ, 697, 824
Andrei, A. H., Smart, R. L., Penna, J. L., et al. 2011, AJ, 141, 54
Artigau, É., Lafrenière, D., Doyon, R., et al. 2011, ApJ, 739, 48
Basri, G., Mohanty, S., Allard, F., et al. 2000, ApJ, 538, 363
Basri, G., & Reiners, A. 2006, AJ, 132, 663
Becklin, E. E., & Zuckerman, B. 1988, Natur, 336, 656
Berriman, B., Kirkpatrick, D., Hanisch, R., Szalay, A., & Williams, R. 2003, in IAU Joint Discussion, 8, 60
Bessell, M. S. 1991, AJ, 101, 662
Billères, M., Delfosse, X., Beuzit, J.-L., et al. 2005, A&A, 440, L55
Blake, C. H., Charbonneau, D., & White, R. J. 2010, ApJ, 723, 684
Blake, C. H., Charbonneau, D., White, R. J., et al. 2008, ApJL, 678, L125
Bochanski, J. J., Hawley, S. L., Covey, K. R., et al. 2010, AJ, 139, 2679
Bochanski, J. J., Hawley, S. L., & West, A. A. 2011, AJ, 141, 98
Boeshaar, P. C., & Tyson, J. A. 1985, AJ, 90, 817
Bouy, H., Brandner, W., Martín, E. L., et al. 2003, AJ, 126, 1526
Bowler, B. P., Liu, M. C., & Dupuy, T. J. 2010, ApJ, 710, 45
Burgasser, A. J. 2007a, ApJ, 659, 655
Burgasser, A. J. 2007b, AJ, 134, 1330
Burgasser, A. J., Bardalez-Gagliuffi, D. C., & Gizis, J. E. 2011a, AJ, 141, 70
Burgasser, A. J., & Blake, C. H. 2009, AJ, 137, 4621
Burgasser, A. J., Cruz, K. L., Cushing, M., et al. 2010a, ApJ, 710, 1142
Burgasser, A. J., Cruz, K. L., & Kirkpatrick, J. D. 2007a, ApJ, 657, 494
Burgasser, A. J., Geballe, T. R., Leggett, S. K., Kirkpatrick, J. D., & Golimowski, D. A. 2006a, ApJ, 637, 1067
Burgasser, A. J., Kirkpatrick, J. D., Brown, M. E., et al. 2002, ApJ, 564, 421
Burgasser, A. J., Kirkpatrick, J. D., Cruz, K. L., et al. 2006b, ApJS, 166, 585
Burgasser, A. J., Liu, M. C., Ireland, M. J., Cruz, K. L., & Dupuy, T. J. 2008a, ApJ, 681, 579
Burgasser, A. J., Looper, D. L., Kirkpatrick, J. D., Cruz, K. L., & Swift, B. J. 2008b, ApJ, 674, 451
Burgasser, A. J., Looper, D., & Rayner, J. T. 2010b, AJ, 139, 2448
Burgasser, A. J., Luk, C., Dhital, S., et al. 2012, ApJ, 757, 110
Burgasser, A. J., Reid, I. N., Siegler, N., et al. 2007b, in Protostars and Planets V, ed. B. Reipurth, D. Jewitt, & K. Keil (Tucson, AZ: Univ. Arizona Press), 427
Burgasser, A. J., Sitarski, B. N., Gelino, C. R., Logsdon, S. E., & Perrin, M. D. 2011b, ApJ, 739, 49
Burningham, B., Leggett, S. K., Lucas, P. W., et al. 2010, MNRAS, 404, 1952
Burrows, A., Marley, M., Hubbard, W. B., et al. 1997, ApJ, 491, 856
Caballero, J. A. 2007, ApJ, 667, 520
Carson, J. C., Marengo, M., Patten, B. M., et al. 2011, ApJ, 743, 141
Casewell, S. L., Jameson, R. F., & Burleigh, M. R. 2008, MNRAS, 390, 1517
Chappelle, R. J., Pinfield, D. J., Steele, I. A., Dobbie, P. D., & Magazzù, A. 2005, MNRAS, 361, 1323
Chiu, K., Fan, X., Leggett, S. K., et al. 2006, AJ, 131, 2722
Choi, J.-Y., Han, C., Udalski, A., et al. 2013, ApJ, 768, 129
Close, L. M., Siegler, N., Freed, M., & Biller, B. 2003, ApJ, 587, 407
Cruz, K., Faherty, J., Rice, E., Riedel, A., & Núñez, A. 2013, in Protostars and Planets VI, Heidelberg, July 15-20, 2013. Poster #2G022, 22
Cruz, K. L., Burgasser, A. J., Reid, I. N., & Liebert, J. 2004, ApJL, 604, L61
Cruz, K. L., Kirkpatrick, J. D., & Burgasser, A. J. 2009, AJ, 137, 3345
Cruz, K. L., Reid, I. N., Kirkpatrick, J. D., et al. 2007, AJ, 133, 439
Cruz, K. L., Reid, I. N., Liebert, J., Kirkpatrick, J. D., & Lowrance, P. J. 2003, AJ, 126, 2421
Cushing, M. C., Marley, M. S., Saumon, D., et al. 2008, ApJ, 678, 1372
Cushing, M. C., Rayner, J. T., Davis, S. P., & Vacca, W. D. 2003, ApJ, 582, 1066
Cushing, M. C., Roellig, T. L., Marley, M. S., et al. 2006, ApJ, 648, 614
Cushing, M. C., Vacca, W. D., & Rayner, J. T. 2004, PASP, 116, 362
Day-Jones, A. C., Marocco, F., Pinfield, D. J., et al. 2013, MNRAS, 430, 1171
Deacon, N. R., Hambly, N. C., & Cooke, J. A. 2005, A&A, 435, 363
Deacon, N. R., Hambly, N. C., King, R. R., & McCaughrean, M. J. 2009, MNRAS, 394, 857

Delfosse, X., Tinney, C. G., Forveille, T., et al. 1999, A&AS, 135, 41
Delgado-Donate, E. J., Clarke, C. J., Bate, M. R., & Hodgkin, S. T. 2004, MNRAS, 351, 617
Dhital, S., Burgasser, A. J., Looper, D. L., & Stassun, K. G. 2011, AJ, 141, 7
Duchêne, G., Bouvier, J., Moraux, E., et al. 2013, A&A, 555, A137
Dupuy, T. J., & Liu, M. C. 2012, ApJS, 201, 19
Dupuy, T. J., Liu, M. C., & Ireland, M. J. 2009, arXiv:0912.0738
EROS Collaboration, Goldman, B., Delfosse, X., et al. 1999, A&A, 351, L5
Faherty, J. K., Burgasser, A. J., Cruz, K. L., et al. 2009, AJ, 137, 1
Faherty, J. K., Burgasser, A. J., Walter, F. M., et al. 2012, ApJ, 752, 56
Fan, X., Knapp, G. R., Strauss, M. A., et al. 2000, AJ, 119, 928
Fischer, D. A., & Marcy, G. W. 1992, ApJ, 396, 178
Folkes, S. L., Pinfield, D. J., Jones, H. R. A., et al. 2012, MNRAS, 427, 3280
Forveille, T., Ségransan, D., Delorme, P., et al. 2004, A&A, 427, L1
Geballe, T. R., Knapp, G. R., Leggett, S. K., et al. 2002, ApJ, 564, 466
Geißler, K., Metchev, S., Kirkpatrick, J. D., Berriman, G. B., & Looper, D. 2011, ApJ, 732, 56
Gelino, C. R., & Burgasser, A. J. 2010, AJ, 140, 110
Gelino, C. R., Kirkpatrick, J. D., Cushing, M. C., et al. 2011, AJ, 142, 57
Gizis, J. E. 2002, ApJ, 575, 484
Gizis, J. E., Monet, D. G., Reid, I. N., Kirkpatrick, J. D., & Burgasser, A. J. 2000a, MNRAS, 311, 385
Gizis, J. E., Monet, D. G., Reid, I. N., et al. 2000b, AJ, 120, 1085
Gizis, J. E., Reid, I. N., Knapp, G. R., et al. 2003, AJ, 125, 3302
Golimowski, D. A., Henry, T. J., Krist, J. E., et al. 2004, AJ, 128, 1733
Hall, P. B. 2002, ApJL, 580, L77
Haro, G., & Chavira, E. 1966, VA, 8, 89
Hawley, S. L., Covey, K. R., Knapp, G. R., et al. 2002, AJ, 123, 3409
Hayashi, C., & Nakano, T. 1963, PThPh, 30, 460
Hwang, K.-H., Udalski, A., Han, C., et al. 2010, ApJ, 723, 797
Irwin, M., McMahon, R. G., & Reid, N. 1991, MNRAS, 252, 61P
Jenkins, J. S., Ramsey, L. W., Jones, H. R. A., et al. 2009, ApJ, 704, 975
Joergens, V. 2008, A&A, 492, 545
Kendall, T. R., Delfosse, X., Martín, E. L., & Forveille, T. 2004, A&A, 416, L17
Kendall, T. R., Jones, H. R. A., Pinfield, D. J., et al. 2007, MNRAS, 374, 445
Kendall, T. R., Mauron, N., Azzopardi, M., & Gigoyan, K. 2003, A&A, 403, 929
Kirkpatrick, J. D. 2005, ARA&A, 43, 195
Kirkpatrick, J. D., Cruz, K. L., Barman, T. S., et al. 2008, ApJ, 689, 1295
Kirkpatrick, J. D., Cushing, M. C., Gelino, C. R., et al. 2011, ApJS, 197, 19
Kirkpatrick, J. D., Henry, T. J., & Simons, D. A. 1995, AJ, 109, 797
Kirkpatrick, J. D., Looper, D. L., Burgasser, A. J., et al. 2010, ApJS, 190, 100
Kirkpatrick, J. D., Reid, I. N., Liebert, J., et al. 1999, ApJ, 519, 802
Kirkpatrick, J. D., Reid, I. N., Liebert, J., et al. 2000, AJ, 120, 447
Knapp, G. R., Leggett, S. K., Fan, X., et al. 2004, AJ, 127, 3553
Kraus, A. L., & Hillenbrand, L. A. 2012, ApJ, 757, 141
Kumar, S. S. 1963, ApJ, 137, 1121
Lépine, S., Rich, R. M., Neill, J. D., Caulet, A., & Shara, M. M. 2002, ApJL, 581, L47
Lépine, S., Rich, R. M., & Shara, M. M. 2003, AJ, 125, 1598
Liebert, J. 1976, PASP, 88, 232
Liebert, J., & Gizis, J. E. 2006, PASP, 118, 659
Liu, M. C., Delorme, P., Dupuy, T. J., et al. 2011, ApJ, 740, 108
Liu, M. C., Dupuy, T. J., Bowler, B. P., Leggett, S. K., & Best, W. M. J. 2012, ApJ, 758, 57
Liu, M. C., Dupuy, T. J., & Leggett, S. K. 2010, ApJ, 722, 311
Lodieu, N., Scholz, R.-D., & McCaughrean, M. J. 2002, A&A, 389, L20
Lodieu, N., Scholz, R.-D., McCaughrean, M. J., et al. 2005, A&A, 440, 1061
Looper, D. L., Gelino, C. R., Burgasser, A. J., & Kirkpatrick, J. D. 2008a, ApJ, 685, 1183
Looper, D. L., Kirkpatrick, J. D., Cutri, R. M., et al. 2008b, ApJ, 686, 528
Luhman, K. L. 2013, ApJL, 767, L1
Luhman, K. L., Mamajek, E. E., Allen, P. R., Muench, A. A., & Finkbeiner, D. P. 2009, ApJ, 691, 1265
Mace, G. N., Kirkpatrick, J. D., Cushing, M. C., et al. 2013, ApJS, 205, 6
Manjavacas, E., Goldman, B., Reffert, S., & Henning, T. 2013, A&A, 560, A52
Martín, E. L., Delfosse, X., Basri, G., et al. 1999, AJ, 118, 2466
Martín, E. L., Phan-Bao, N., Bessell, M., et al. 2010, A&A, 517, A53
McElwain, M. W., & Burgasser, A. J. 2006, AJ, 132, 2074
Metchev, S. A., Kirkpatrick, J. D., Berriman, G. B., & Looper, D. 2008, ApJ, 676, 1281
Padoan, P., & Nordlund, Å. 2002, ApJ, 576, 870
Phan-Bao, N. 2011, AN, 332, 668
Phan-Bao, N., Bessell, M. S., Martín, E. L., et al. 2008, MNRAS, 383, 831
Phan-Bao, N., Crifo, F., Delfosse, X., et al. 2003, A&A, 401, 959
Pinfield, D. J., Dobbie, P. D., Jameson, R. F., et al. 2003, MNRAS, 342, 1241
Pokorny, R. S., Jones, H. R. A., Hambly, N. C., & Pinfield, D. J. 2004, A&A, 421, 763
Radigan, J., Jayawardhana, R., Lafrenière, D., et al. 2013, ApJ, 778, 36
Radigan, J., Lafrenière, D., Jayawardhana, R., & Doyon, R. 2008, ApJ, 689, 471
Rayner, J. T., Toomey, D. W., Onaka, P. M., et al. 2003, PASP, 115, 362
Rebolo, R., Zapatero Osorio, M. R., Madruga, S., et al. 1998, Sci, 282, 1309
Reid, I. N., Cruz, K. L., Kirkpatrick, J. D., et al. 2008, AJ, 136, 1290
Reid, I. N., & Gizis, J. E. 2005, PASP, 117, 676
Reipurth, B., & Clarke, C. 2001, AJ, 122, 432
Ruiz, M. T., & Takamiya, M. Y. 1995, AJ, 109, 2817
Sahlmann, J., Lazorenko, P. F., Ségransan, D., et al. 2013, A&A, 556, A133
Salim, S., Lépine, S., Rich, R. M., & Shara, M. M. 2003, ApJL, 586, L149
Schmidt, S. J., West, A. A., Hawley, S. L., & Pineda, J. S. 2010, AJ, 139, 1808
Schneider, A. C., Cushing, M. C., Kirkpatrick, J. D., et al. 2014, AJ, 147, 34
Schneider, D. P., Knapp, G. R., Hawley, S. L., et al. 2002, AJ, 123, 458
Scholz, R.-D. 2010, A&A, 510, L8
Scholz, R.-D. 2014, A&A, 561, A113
Scholz, R.-D., Lodieu, N., & McCaughrean, M. J. 2004, A&A, 428, L25
Scholz, R.-D., Meusinger, H., & Jahreiß, H. 2001, A&A, 374, L12
Scholz, R.-D., Storm, J., Knapp, G. R., & Zinnecker, H. 2009, A&A, 494, 949
Shkolnik, E., Liu, M. C., & Reid, I. N. 2009, ApJ, 699, 649
Shkolnik, E. L., Anglada-Escudé, G., Liu, M. C., et al. 2012, ApJ, 758, 56
Shu, F. H., Adams, F. C., & Lizano, S. 1987, ARA&A, 25, 23
Stamatellos, D., & Whitworth, A. P. 2009, MNRAS, 392, 413
Stumpf, M. B., Brandner, W., Bouy, H., Henning, T., & Hippler, S. 2010, A&A, 516, A37
Stumpf, M. B., Brandner, W., Henning, T., et al. 2008, arXiv:0811.0556
Stumpf, M. B., Geißler, K., Bouy, H., et al. 2011, A&A, 525, A123
Thompson, M. A., Kirkpatrick, J. D., Mace, G. N., et al. 2013, PASP, 125, 809
Tinney, C. G., Delfosse, X., Forveille, T., & Allard, F. 1998, A&A, 338, 1066
Tinney, C. G., Mould, J. R., & Reid, I. N. 1993, AJ, 105, 1045
Vacca, W. D., Cushing, M. C., & Rayner, J. T. 2003, PASP, 115, 389
van Biesbroeck, G. 1961, AJ, 66, 528
West, A. A., Hawley, S. L., Bochanski, J. J., et al. 2008, AJ, 135, 785
West, A. A., Morgan, D. P., Bochanski, J. J., et al. 2011, AJ, 141, 97
Whitworth, A. P., & Zinnecker, H. 2004, A&A, 427, 299
Wilson, J. C., Kirkpatrick, J. D., Gizis, J. E., et al. 2001, AJ, 122, 1989
Wilson, J. C., Miller, N. A., Gizis, J. E., et al. 2003, in IAU Symp. 211, Brown Dwarfs, ed. E. Martín (San Francisco, CA: ASP), 197
York, D. G., Adelman, J., Anderson, J. E., Jr., et al. 2000, AJ, 120, 1579
Zhang, Z. H., Pinfield, D. J., Day-Jones, A. C., et al. 2010, MNRAS, 404, 1817
Zhang, Z. H., Pokorny, R. S., Jones, H. R. A., et al. 2009, A&A, 497, 619